

Durham Research Online

Deposited in DRO:

25 June 2018

Version of attached file:

Accepted Version

Peer-review status of attached file:

Peer-reviewed

Citation for published item:

O'Regan, M. and Coxall, H. and Hill, P. and Hilton, R. and Muschitiello, F. and Swärd, H. (2018) 'Early Holocene sea level in the Canadian Beaufort Sea constrained by radiocarbon dates from a deep borehole in the Mackenzie Trough, Arctic Canada.', *Boreas*, 47 (4). pp. 1102-1117.

Further information on publisher's website:

<https://doi.org/10.1111/bor.12335>

Publisher's copyright statement:

This is the accepted version of the following article: O'Regan, M., Coxall, H., Hill, P., Hilton, R., Muschitiello, F. Swärd, H. (2018). Early Holocene sea level in the Canadian Beaufort Sea constrained by radiocarbon dates from a deep borehole in the Mackenzie Trough, Arctic Canada. *Boreas* 47(4): 1102-1117, which has been published in final form at <https://doi.org/10.1111/bor.12335>. This article may be used for non-commercial purposes in accordance With Wiley Terms and Conditions for self-archiving.

Use policy

The full-text may be used and/or reproduced, and given to third parties in any format or medium, without prior permission or charge, for personal research or study, educational, or not-for-profit purposes provided that:

- a full bibliographic reference is made to the original source
- a [link](#) is made to the metadata record in DRO
- the full-text is not changed in any way

The full-text must not be sold in any format or medium without the formal permission of the copyright holders.

Please consult the [full DRO policy](#) for further details.

Early Holocene sea level in the Canadian Beaufort Sea constrained by radiocarbon dates from a deep borehole in the Mackenzie Trough, Arctic Canada

MATT O'REGAN, HELEN COXALL, PHILIP HILL, ROBERT HILTON, FRANCESCO MUSCHITIELLO AND HENRIK SWÄRD

Deglacial and Holocene relative sea level (RSL) in the Canadian Beaufort Sea was influenced by the timing and extent of glacial ice in the Mackenzie River corridor and adjacent coastal plains. Considerable evidence indicates extensive ice cover in this region of northwestern Canada during the Late Wisconsinan. However, no absolute ages exist to constrain maximum RSL lowering before the late Holocene (4.2-0 ka). In 1984, the Geological Survey of Canada drilled an 81.5 m-deep borehole in the western Mackenzie Trough at 45 m water depth (MTW01). The lower 52.5 m of the borehole were interpreted as a deltaic progradational sequence deposited during a period of rising sea level. The upper 29 m were described as foraminifer-bearing marine sediments deposited after transgression of the site, when RSL rose above ~ -74 m. Here we present radiocarbon measurements from MTW01, acquired from benthic foraminifera, mollusc fragments and particulate organic carbon in the $>63 \mu\text{m}$ fraction ($\text{POC}_{>63\mu\text{m}}$) in an attempt to constrain the chronology of sediments within this borehole and date the timing of transgression. The deepest carbonate macrofossil was acquired from 8 m above the transgressive surface (equivalent to 21 m b.s.l.), where mollusc fragments returned a date of 9400 ± 180 cal. a BP (2σ). This provides the oldest constraint on Holocene sea-level lowering in the region, and implies that transgression at this site occurred prior to the early Holocene. Ages obtained from the lower 52.5 m of the borehole are limited to $\text{POC}_{>63\mu\text{m}}$ samples. These indicate that progradational sediments were deposited rapidly after $24\,820 \pm 390$ cal. a BP (2σ). Due to the incorporation of older reworked organic matter, the actual age of progradation is likely to be younger, occurring after Late Wisconsinan glacial ice retreated from the coast.

KEYWORDS: Holocene, Mackenzie Trough, radiocarbon, sea level

Matt O'Regan (matt.oregan@geo.su.se), Helen Coxall (helen.coxall@geo.su.se) and Henrik Swärd (henrik.sward@geo.su.se), Department of Geological Sciences, Stockholm University, Svante Arrhenius väg 8, 10691, Stockholm, Sweden; Philip Hill (Philip.Hill@NRCan-RNCan.gc.ca), Geological Survey of Canada-Atlantic, Pacific Geosciences Center, 9860 West Saanich Road, Sydney, British Columbia, V8L 4B2, Canada; Francesco Muschitiello (francesco.muschitiello@geog.cam.ac.uk), Department of Geography, University of Cambridge, Downing Place, Cambridge, CB2 3EN, United Kingdom; Robert Hilton (R.G.Hilton@durham.ac.uk), Durham University, Department of Geography, Lower Mountjoy South Road, Durham, DH1 3LE, United Kingdom.

The Mackenzie Trough (MT) is a ~130 km long, 75 km wide glacially excavated cross-shelf trough in the western Canadian Beaufort Sea (Shearer 1971; Rampton 1982; O'Connor 1989; Blasco *et al.* 1990; Batchelor *et al.* 2013a) (Fig. 1). Lying at the northwestern limit of the Laurentide Ice Sheet (LIS), the region was dramatically affected by glacial and periglacial processes during the Quaternary (Rampton 1982, 1988; Dyke & Prest 1987; Murton *et al.* 2007; Fritz *et al.* 2012; Jakobsson *et al.* 2014). Constraining the extent and timing of glacial advances into the Mackenzie delta region is important to understand variations in the long-term delivery of freshwater, suspended sediment and organic material into the Arctic Ocean (Macdonald *et al.* 1988; Hilton *et al.* 2015; Wegner *et al.* 2015; McClelland *et al.* 2016). It is also necessary for assessing how eustatic and glacioisostatic changes in sea level affected permafrost, gas hydrate, and landscape development of the eastern Beaufort Sea margin (Taylor *et al.* 2013), and for interpreting regional offshore seismic stratigraphy (Blasco *et al.* 1990; Batchelor *et al.* 2013a, b). The regional deglacial history is also of particular interest, as a freshwater outburst from Glacial Lake Agassiz routed to the Arctic via the Mackenzie River, remains a controversial but plausible triggering mechanism for the Younger Dryas cold period (~12.9 to 11.7 cal. ka BP; Rasmussen *et al.* 2006) (Tarasov & Peltier 2005; Peltier *et al.* 2006; Murton *et al.* 2010; Condon & Windsor 2012). Unravelling this interplay between glacial activity, sea-level change and variations in Mackenzie River discharge requires the integration of dated marine and terrestrial archives from the Beaufort Sea region.

Within the Mackenzie River delta region, terrestrial glacial landforms delineate two advances of the LIS during the last glacial cycle (Marine Isotope Stage 4-2, or the

Wisconsinan Glaciation) that inundated the Yukon coastal plain (Bostok 1948; Rampton 1982; Hughes 1987; Rampton 1988). The older of these is called the Toker Point Stade along the Tuktoyaktuk Peninsula, and the Buckland glaciation along the Yukon coastal plain (Rampton 1982, 1988) (Fig. 1). During this time, glacial landforms and striations indicate a lobe of northwestern flowing ice in the Mackenzie River corridor (named the Mackenzie ice stream by Stokes *et al.* 2006) that spread across the Yukon coastal plain, Richards Island and the southwestern end of the Tuktoyaktuk Peninsula (Fig. 1). Glacial drift mapped along the Richardson and British mountains, suggest ice thicknesses of 300-900 m, rapidly thinning towards its western limit north of Herschel Island (Rampton 1982; Beget 1987). The offshore limits of this advance are generally poorly mapped, and its position remains speculative (Fig.1). Within the limits of the Toker Point Stade, well-preserved moraines and other ice-marginal features delineate a secondary, less extensive advance or stillstand of the Mackenzie ice stream known as the Sitidgi Stade or Tutsieta Lake Phase (Hughes 1987; Rampton 1988) (Fig. 1).

Radiocarbon dates on wood fragments from within the Toker Point outwash (Rampton 1988; Vincent 1989, 1992), and shell fragments in sediments overlying Toker Point till (Mackay *et al.* 1972), initially indicated an Early Wisconsinan age (MIS 5-4) for the earlier, more extensive ice advance. As a result, there was a long-standing view that the Sitidgi Stade represented a limited glacial advance during the Late Wisconsinan (MIS 2) (Beget 1987; Vincent & Prest 1987; Rampton 1982; Dyke *et al.* 2002; Dyke 2004). Subsequently, luminescence dating of aeolian dune sands (the Kittigazuit Formation) pre-dating the Toker Point till on the Tuktoyaktuk Peninsula (Fig. 1), constrained the Toker Point Stade to between ~22 and 16 cal. ka

95 BP (Murton *et al.* 2007).

96

97 This Late Wisconsinan age for the Toker Point Stade is further supported by
98 U/Th dates on calcite concretions recovered from aufeis buried by glacial till in the
99 Peel Plateau region of the Richardson mountains in the Northwest Territories
100 (67°07.75' N; 135 °55.74' W) (Lacelle *et al.* 2013). These dates indicate that the
101 arrival of glacial ice occurred after 18.5 cal. ka BP (Lacelle *et al.* 2013). Farther north,
102 radiocarbon dating on vascular plant detritus in ice thrust sediments on Herschel
103 Island (Fig. 1), also indicate the arrival of glacial ice after 16.2±6 (2σ) cal. ka BP
104 (Fritz *et al.* 2012). Although no absolute ages constrain the beginning of the Sitidgi
105 Stade, radiocarbon dates obtained on grasses from sandy outwash in the Eskimo
106 Lakes (Fig. 1) date the Sitidgi glacial maximum to the Late Wisconsinan, ~13 ¹⁴C ka
107 BP (~15 – 16 cal. ka BP) (Rampton 1988; Murton *et al.* 2007). Therefore, the current
108 view is that the Toker Point and Sitidgi Stade occurred in close succession during the
109 Late Wisconsinan (MIS 2), and that the Sitidgi Stade was a short-lived re-advance or
110 standstill during the deglacial retreat of the Mackenzie ice stream (Murton *et al.*
111 2007). A more extensive Late Wisconsinan advance of the LIS into the Beaufort Sea
112 is consistent with revised glacial extents farther to the east, which also show that
113 during MIS 2, glacial ice extended across Banks Island (England *et al.* 2009;
114 Lakeman & England 2012, 2013), which had previously been portrayed as being ice
115 free during the Last Glacial Maximum (LGM) (Dyke *et al.* 2004).

116

117 Before the widespread acceptance of an extensive Late Wisconsinan ice
118 advance, a relative sea level (RSL) curve for the Beaufort shelf was constructed (Hill
119 *et al.* 1985, 1993). This was achieved using a compilation of radiocarbon ages

obtained from offshore boreholes and sediment cores containing peat or shell samples whose composition and/or stratigraphic position indicated deposition either above (minimum sea-level lowering) or below (maximum sea-level lowering) palaeo-sea level (Fig. 2, Table 1) (Hill *et al.* 1985, 1993). Prior to ~4 cal. ka BP, the existing data only provide minimum estimates of sea-level lowering, leaving considerable uncertainty in RSL during deglaciation and the early Holocene (defined as 11.7 - 8.2 cal. ka BP by Walker *et al.* 2012) (Hill *et al.* 1993; Hill 1996). The inferred RSL changes predating radiocarbon constraints were derived by combining observations on the depth of incised channels on the Beaufort Shelf, argued to have formed during a RSL lowstand during the Sitidgi Stade, with estimates of the glacioisostatic effects resulting from restricted Late Wisconsinan ice sheet cover (Hill *et al.* 1985, 1993; Hill 1996) (Fig. 2). Formation of the incised channels have more recently been interpreted as a response to a glacial outburst flood during the Younger Dryas (Murton *et al.* 2010).

An important sedimentary archive, containing potential deglacial to early Holocene relative sea-level constraints, and a record of fluvial sedimentation and evolution of the Holocene Mackenzie River delta, is the 81.5 meter-long MTW01 borehole (Fig. 1). MTW01 was drilled by the Geological Survey of Canada in 1984 in the western Mackenzie Trough at 45 m water depth. A 71 m piezocone penetrometer profile was also acquired at an offset site 50 m away, which provided continuous insitu sedimentological characterization (Moran *et al.* 1989) (Fig. 3). Five sedimentary units were defined in MTW01 (A to E) (Fig. 3) (Moran *et al.* 1989), integrated with seismic data, and placed into a sequence stratigraphic framework for the delta front and upper trough area (Moran *et al.* 1989; Hill 1996) (Fig. 3).

A transgressive surface of erosion is located at 29 m b.s.f. (74 m b.s.l.). It comprises the contact between Units B and C, where the underlying Units C, D, and E are interpreted as a deltaic progradational sequence of a transgressive systems tract (i.e. deposited during a rising RSL) (Moran *et al.* 1989; Hill 1996). Within MTW01, Unit B directly overlies the inundation surface, and is a 9 m sequence of laminated and in parts deformed silt and clay, that coarsens into interbedded sands, silts and clays near the top (Fig. 3) (Moran *et al.* 1989; Hill 1996). It is interpreted as a transitional unit formed after the early stages of transgression, prior to the deposition of bioturbated, foraminifer bearing marine clays of Unit A (Moran *et al.* 1989; Hill 1996). In seismic data, Units A and B are separated by a disconformable reflector, which becomes conformable moving seaward (Fig. 3) (Moran *et al.* 1989).

No absolute ages exist from MTW01 to date the period of progradation or the timing of local transgression at the borehole site. Units E-C reportedly contain large numbers of reworked pre-Quaternary to Quaternary palynomorphs, and marine algae, with abundant pollen. The composition of the palynomorph assemblages was reported to be compatible with deposition during approximately the last 14 cal. ka BP (Blasco *et al.* 1990). Unit B is dominated by a terrestrial pollen assemblage containing *Cyperaceae*, *Gramineae*, *Sphagnum* and an up-core increase in *Pediastrum* (Blasco *et al.* 1990). A dominance of *Picea* in the marine clays at the base of Unit A was used to assign an age of 9.5 cal. ka BP for the base of this unit, with an *Alnus* peak at 11.5 m suggesting an age of 6.8 cal. ka BP (Blasco *et al.* 1990) (Fig. 3).

The absence of absolute ages for the sediments within MTW01 leaves

considerable uncertainty regarding the age and significance of the transgressive surface of erosion and the timing of delta progradation with respect to ice sheet retreat. For example, in the supplementary information of Murton *et al.* (2010), it is suggested that the unconformity lying on top of the progradational sequence in MTW01 (separating Units C and B) may have developed in response to fluvial erosion during a glacial outburst flood at the start of the Younger Dryas (when RSL was -70 to -80 m), and was later buried by marine sediments during transgression (Fig. 3). These competing interpretations, erosion in response to either shelf transgression, or fluvial activity at the onset of the Younger Dryas, could be tested through better dating of the sediments in the MTW01 borehole.

In this study we revisited archived samples from MTW01 to find suitable material for radiocarbon dating in an attempt to: i) date the timing of delta progradation; ii) identify the stratigraphic position of the Younger Dryas within the borehole; and iii) provide an absolute RSL constraint for the Beaufort Sea during deglaciation or the early Holocene. The absence of marine macrofossils and calcareous microfossils below the uppermost sediment within Unit B prevents us from accomplishing the first 2 objectives. However, the occurrence of terrestrial organic matter in these sediments helps us to constrain a maximum age for these deposits and assess the rate of sedimentation. In contrast, the continuous occurrence of foraminifera and mollusc fragments in sediments above 22 m b.s.f. allows us to reconstruct Holocene sedimentation rates at this site, and provide further early Holocene relative sea-level constraints for the Beaufort Sea Shelf.

Methods

The MTW01 borehole was drilled from a 114-m long barge (*Arctic Kiggiak*) converted for geotechnical fieldwork (Moran *et al.* 1989). Spot (intermittent) samples from the borehole were collected at intervals of 1 to 3 m, and were 0.3 to 0.8 m in length. While no intact core sections remain, subsamples of the cores are stored as dried bag samples and are stored at room temperature at the GSC-Atlantic core repository. These samples were originally taken for geotechnical investigations. In some instances, these bag samples contain material from decimeter-scale sections of the original core. Therefore in terms of sample thickness they range from 2-60 cm in length. Subsamples were taken from 26 of these bag samples, and ranged in weight from 50-100 g of dry sediment.

Between 27 and 90 g of each sample were wet sieved through a 38 μm sieve and dried at 48 °C for 24 hours. The fine fraction material was collected, also dried at 48 °C for 24 hours, weighed and stored for future use. The >38 μm fractions were spilt, using a particle microsplitter, by factors of 8-32 (depending on sample size) to provide manageable amounts of material for microfossil counting. For each split, the >38 μm fraction was further separated using a 63 μm sieve. Quantitative counts of intact benthic and planktic foraminifera, and foraminifera, ostracod and bivalve fragments, were made on each split sample in the >63 μm size range. The purpose was to record the distribution of calcareous microfossil/macrofossil material in the core and identify horizons with sufficient material for dating. Detailed assemblage counts were not made on these samples.

Based on the down-core counting, five foraminifera-rich samples were selected for radiocarbon dating. The dates were generated from mixed benthic

foraminifera, which were far more abundant than planktics. The five samples contained similar benthic foraminifera assemblages. The most common species were the shallow infaunal taxon *Elphidium excavatum* subsp. *clavatum*, *Cassidulina reniformis* and *Bulivina arctica*. *Cassidulina teretis* was also common in samples 1A, 6B and 12B, but scarce in the stratigraphically lower samples (14B and 15B). Approximately 400-600 individuals were picked from the >63 μm size fraction in each of these samples. In three additional samples, millimeter sized mollusc fragments were picked for independent dating. The fragments were too small to allow species identification but were likely from the same species of bivalve molluscs. Each mollusc fragment sample comprised multiple millimeter-sized fragments (5-10 pieces per sample) in order to obtain the sample weights required for dating. Representative mollusc fragments and foraminifera were imaged using a Leica M205 C light microscope and camera system. The foraminifer and mollusc fragment samples were sent to the National Ocean Sciences Accelerator Mass Spectrometry Facility (NOSAMS) at Woods Hole Oceanographic Institution for ^{14}C analysis.

A further 10 samples were processed in order to measure the ^{14}C activity of particulate organic matter. Bulk samples were wet sieved at 63 μm , dried, and homogenised in an agate pestle and mortar. Marine sediments proximal to rivers with high erosion rates and sedimentary rocks in their upland basin are known to contain important components of rock-derived organic carbon (Blair *et al.* 2003; Galy *et al.* 2008; Kao *et al.* 2014). This is also the case in the Mackenzie River basin and for adjacent offshore sediments, where fluvial erosion and transport of unlithified Neogene and Quaternary sediments are known to contribute significantly to organic matter deposition (Rampton 1988; Goni *et al.* 2005, 2013). In the modern Mackenzie

river, rock derived organic carbon has been shown to be more important in the clay-silt fraction, whereas plant detritus tends to be more prevalent in the coarser fractions (Hilton *et al.* 2015). Therefore, the $>63 \mu\text{m}$ fraction of particulate organic carbon ($\text{POC}_{>63\mu\text{m}}$) was targeted for dating. We acknowledge that soil-derived POC in the modern Mackenzie River is significantly aged (Goni *et al.* 2005; Hilton *et al.* 2015) and that rock-derived POC may still be present in this size fraction, and so interpretation of the ^{14}C activity of these samples solely in terms of depositional chronology may be difficult.

Sieved sediment samples were subject to HCl fumigation in order to remove inorganic carbon and avoid loss of a component of POC (Komada *et al.* 2008; Whiteside *et al.* 2011). Aliquots ($\sim 1 \text{ g}$) of homogenised sample were placed in clean glass vials in an evacuated desiccator containing $\sim 50 \text{ mL}$ 12N HCl in an oven and heated between 60 and 65 $^{\circ}\text{C}$ for 60 to 72 hours. Samples were transferred to another vacuum desiccator charged with indicating silica gel, pumped down and dried to remove HCl fumes. Acidified aliquots were prepared to graphite at the NERC Radiocarbon Facility of between 1-2 mg C for each sample and standard. ^{14}C activity was measured by Accelerator Mass Spectrometry at the Scottish Universities Environmental Research Centre. Process standards (96H humin) and background materials (bituminous coal) were taken through all stages of sample preparation and ^{14}C analysis and were within 2σ uncertainty of expected values. Stable isotopes of POC ($\delta^{13}\text{C}$) were measured by dual-inlet isotope ratio mass spectrometer (IRMS) on an aliquot of the same CO_2 .

Radiocarbon dates for the benthic foraminifera and mollusc fragment samples were converted to calibrated ages with the Marine13 calibration curve (Reimer *et al.* 2013) using CLAM (Blaauw 2010). A ΔR of 335 ± 85 years was applied, and is based on a recent re-analysis of ages from 24 living mollusc specimens collected before 1956 from the northwestern Canadian Arctic Archipelago (Coulter *et al.* 2010). This sample set does not include specimens from the Beaufort Sea and as such only provides a best estimate for ΔR in the Mackenzie Trough. No reservoir correction was applied to the $\text{POC}_{>63\mu\text{m}}$ samples, where calibrated ages were returned using the IntCal13 dataset (Reimer *et al.* 2013). All calibrated ages are rounded to the nearest decade, and reported with the 95.4% (2σ) confidence interval.

The new radiocarbon ages from MTW01 are compared to a compilation of radiocarbon-dated samples used to construct the Holocene RSL curve for the Beaufort Sea (Hill *et al.* 1985, 1993; Hill 1996) (Fig. 2). Radiocarbon ages reported in these earlier studies were calibrated using the updated Marine13 and IntCal13 datasets (Reimer *et al.* 2013), and for consistency, a ΔR of 335 ± 85 years was applied.

Results

Trends in grain size reflect the initial descriptions from borehole sediment and piezocone penetrometer analysis (Moran *et al.* 1989) (Fig. 4). Unit A is dominated by silty clays, with an average of $1.5 \pm 0.4\%$ wt in the $>38 \mu\text{m}$ size fraction, Unit B is slightly coarser ($2.1 \pm 1.2\%$ wt), while the deltaic sediments of Units C through E have a highly variable but coarser texture ($29.6 \pm 19.49\%$ wt $>38 \mu\text{m}$). Rare to common abundances of pollen, fibrous organic material and woody fragments were qualitatively noted in all samples.

The stratigraphically lowest foraminifera and mollusc-rich horizon was 22.56-22.85 m b.s.f. (sample 17B, Unit B) (Fig. 4). This sample contained small numbers of planktic foraminifera, as well as foraminifera and ostracod fragments. All samples above this level contained calcareous biogenic material (Fig. 4). When normalized to the dry weight of the bulk sample, the abundance of calcareous biogenic material is relatively low due to the dominance of fine-grained terrigenous material (Fig. 4). Benthic foraminifera first appear at 21.64-21.99 m b.s.f. (Unit B) (sample 16B) in generally low numbers (12 g^{-1} dry sediment), with an order of magnitude increase in abundance by 20.73-21.09 m b.s.f. (Unit A) (sample 15B) (Fig. 4). The foraminiferal calcite is well preserved as revealed by the shiny, transparent tests (Fig. S1). However, discoloration of some tests implies authigenic infillings do occur.

Bivalve fragments are present within all samples starting at 21.64-21.99 m b.s.f. (sample 16B, Unit B). These fragments were generally 1-2 mm in size and too small for species identification (Fig. 5). Most retained some of the periostracum, a thin organic coating forming the outermost layer of the shell (Fig. 6). Although heavily fragmented, the existence of the periostracum, which is easily eroded by chemical and physical weathering, suggests moderate preservation, with some fragments (Fig. 5A) appearing better preserved than others (Fig. 5C). We cannot rule out that these fragments have undergone some limited transport, or that the fragments represent specimens of varying age.

To investigate the potential affects of reworking on the mollusc fragment ages, paired measurements of benthic forams and mollusc fragments were performed at 2

intervals (0.00-0.20 and 7.62-8.12 m b.s.f.) (samples 1A and 6B). The median calibrated ages of the mollusc fragment samples are 290 and 470 years younger than the benthic foram samples, but the calibrated age distributions do overlap at 2σ (Table 2, Fig. 6). The mollusc fragment sample from 16B (Unit B, 21.64-21.99 m b.s.f.) provided the deepest reliable radiocarbon age for sediments in the borehole (9400^{+180}_{-260} cal. a BP) (Table 2, Fig. 6). Across the Unit A/B boundary, an age offset of 740 years exists between the median calibrated age of the mollusc fragment sample at 21.64-21.99 m b.s.f. (9400^{+180}_{-260} cal. a BP, 16B), and the benthic foraminifera sample at 20.73-21.09 m b.s.f. (8660^{+300}_{-260} cal. a BP, 15B) (Fig. 6). These calibrated ages do not overlap at 2σ . The youngest ages (1080^{+180}_{-170} cal. a BP for the mollusc fragment sample, and 790^{+160}_{-150} cal. a BP for the benthic foraminifera sample), acquired from the top of the borehole (1A, 0-0.2 m b.s.f.), suggest that modern sediments were not recovered (Table 2). This may either reflect a lack of modern deposition, or incomplete recovery of unconsolidated seafloor sediments.

An important observation concerning all the radiocarbon results from foraminifera and mollusc fragment samples, is that no reversals exist in the calibrated ages (at the 95% confidence level) within the marine silts and clays of Unit A (Figs. 6, 7). To account for differences in the radiocarbon ages returned by the paired benthic foraminifer and mollusc fragment samples, and to provide a best estimate for the ages at these depths, an age-depth model was generated with CLAM (Blaauw 2010). The model was based on linear-interpolation through the calibrated probability distributions of the age-depth points from Unit A (Table 2, Fig. 6). Due to the existence of a possible hiatus between Units A and B, the linear-interpolation model is not extended across this stratigraphic boundary. Modelled minimum/maximum

estimates of sample ages for Unit A are provided based on the 2σ range at the top and base of each sample interval (Table 2). By definition, the interpolated age model introduces changes in sedimentation rate at each of the age-depth markers (Fig. 6). Due to the low sampling resolution, these may or may not accurately reflect the true nature of deposition. For discussion purposes, a more conservative average linear sedimentation rate of $2.65 \pm 0.06 \text{ m ka}^{-1}$ ($r^2 = 0.997$) is defined using the modelled best estimate for all samples in Unit A (0-21.09 m b.s.f.). This relatively rapid sedimentation rate is consistent with high Holocene accumulation rates observed in sediment cores from farther offshore in the Mackenzie Trough (Bringue & Rochon 2012; Schell *et al.* 2008) and on the adjacent slope (Andrews & Dunhill 2004).

In the upper 21 m of the borehole (Unit A), the average offset between $\text{POC}_{>63\mu\text{m}}$ ages and benthic foraminifera or mollusc fragment samples is $8400 \pm 850 \text{ }^{14}\text{C a BP}$ (Fig. 7). They range from $7710 \pm 65 \text{ }^{14}\text{C a BP}$ (sample 6B) to $9950 \pm 110 \text{ }^{14}\text{C a BP}$ (sample 12B) and are larger near the base of the unit (Fig. 7). These offsets are remarkably similar to the bulk $\text{POC }^{14}\text{C}$ age measured in the suspended load sediments of the modern day Mackenzie River (sampled at the modern delta), with an average age of $7563 \pm 1420 \text{ }^{14}\text{C a BP}$ ($n = 8$, \pm standard deviation) (Hilton *et al.* 2015). The ^{14}C -depletion of organic matter in the Mackenzie River is mainly attributed to the erosion of old soil from peatlands, with additional contributions from rock-derived organic carbon (Hilton *et al.* 2015). The smaller offsets in the younger two samples coincide with more positive $\delta^{13}\text{C}$ values, and may thus partly be explained by a greater proportion of contemporaneous marine-derived organic carbon, which likely has greater ^{14}C activity than fluvially reworked terrestrial organic matter.

The deepest sample (43B, 81.08 - 81.50 m b.s.f.) from the progradational facies (Units E-C) returned the youngest age from this sequence, $20\,606 \pm 118$ ^{14}C a BP ($24\,820 \pm_{380}^{390}$ cal. a BP) (Table 3, Fig. 6). An apparent difference in calibrated age of 2360 years exists between the median calibrated age of this sample and the lowermost $\text{POC}_{>63\mu\text{m}}$ age from Unit B ($22\,460 \pm_{210}^{260}$ cal. a BP) (Table 3, Fig. 6). An apparent age difference of 1750 years exists in the median calibrated $\text{POC}_{>63\mu\text{m}}$ age between the base of Unit B (sample 21B) and the base of Unit A (sample 15B).

Discussion

Foraminifera and mollusc fragment ages

The occurrence and abundance of calcareous biogenic material in the analysed samples only permits absolute dating from the top of Unit B and above (Fig. 6). Furthermore, the deepest absolute date for the sequence comes from mollusc shell fragments (Fig. 6). England *et al.* (2013) documented a significant bias in radiocarbon ages derived from deposit feeding molluscs (i.e. *Portlandia arctica*) when compared to suspension feeding species. This bias is most pronounced when deposit-feeding molluscs are found within calcareous sediments, with reported age offsets of up to 2 ^{14}C ka (England *et al.* 2013). The mollusc shell fragments dated in this study are too small to allow species identification, but the younger ages found for the analysed fragments, compared to the paired mixed benthic foraminifera dates, suggests that *Portlandia* fragments were absent from the sample set.

Anomalously older radiocarbon ages from foraminifera samples compared to those from corresponding mollusc fragments at the same stratigraphic level, are best explained by a combination of factors: i) redeposition (i.e. mixing) of older benthic

foraminifera in the samples (i.e. Heier-Nielsen *et al.* 1995); ii) partial shell dissolution, the incorporation of other fine-grained carbonaceous sediment trapped within the foram tests, or post-depositional organic linings that incorporate old carbon and would bias the ^{14}C measurements towards older ages (i.e. Mekik 2014; Heier-Nielsen *et al.* 1995); iii) the sample thickness, which was 20 cm for the shallowest (1A, 0.00-0.20 m b.s.f.) and 50 cm for deepest paired measurement (6B, 7.62-8.12 m b.s.f.). Given the average sedimentation rate of $2.65 \pm 0.06 \text{ m ka}^{-1}$, these sample intervals would correspond to ~75 years for sample 1A and ~188 years for sample 6B. These age ranges could only account for part of the offsets seen between these samples (1A - 280 years; 6B - 470 years), but is nonetheless significant.

In summary, the small size of the mollusc fragments prevents us from identifying them to the species level. The small fragments suggest that they are to some degree reworked, unless they were mechanically crushed during geotechnical sample testing in the 1980's. However, the overlapping calibrated ages (2σ) between the mollusc fragment samples and the paired benthic foraminifera samples suggest that they still provide reliable dates. Numerous possible explanations exist to account for the observed offsets in the paired measurements, including the thickness of the sampling intervals. Given that no age reversals exist in the calibrated ages from the foraminifera and mollusc fragments throughout Unit A and B, we suggest that the mollusc fragment sample from the top of Unit B is also a reliable radiocarbon date (Fig. 6) that can be used to constrain the timing of marine transgression at the site.

Relative sea level in the early Holocene

The mixed mollusc fragment sample from the top of Unit B at 21.64-21.99 m b.s.f.

(16B), and the benthic foraminifera sample from the base of Unit A at 20.73-21.09 m b.s.f. (15B) provide important constraints for RSL in the early Holocene. The current water depth of 45 m b.s.l for the site place these samples at 65.73-66.09 m b.s.l (~66 m b.s.l) and 64.81-65.22 m b.s.l (~65 m b.s.l) respectively (Fig. 6). As these were deposited in a marine setting, they imply that sea level was higher than -66 m by 9400⁺¹⁸⁰₋₂₆₀ cal. a BP using the mollusc fragment sample (16B) and higher than -65 m by 8660⁺³⁰⁰₋₂₆₀ cal. a BP based on the mixed benthic foraminifera sample (15B) (Fig. 6). These ages are the oldest constraints for the magnitude of the Holocene transgression in the region. Our new results show RSL was ~34 m lower than the modelled the modeled contemporaneous (9400 cal. a BP) global mean sea level (-32 m) (Lambeck *et al.* 2014; Fig. 8), highlighting the effects of glacial isostatic adjustments (GIA) and other factors on Holocene RSL on the Beaufort Sea Shelf. The new RSL constraint remains consistent with evidence of expanded LIS margins and greater glacioisostatic loading during the Late Wisconsinan (Bateman & Murton, 2006; Murton *et al.* 2007; England *et al.* 2009; Murton *et al.* 2010; Fritz *et al.* 2012; Lakeman & England 2012, 2013).

The new data support the average inferred sea-level curve presented by Hill *et al.* (1993) from 9-10 cal. ka BP, and assuming that our ΔR correction is correct, considerably reduce the uncertainty in the estimate of RSL at this time (Fig. 8). For the subsequent early and middle Holocene, the resulting data-generated RSL curve from Hill *et al.* (1993) is strongly constrained by five offshore boreholes, with three previously published dates from terrestrial facies (#16, #8, #3, Table 1) and two previously published dates from marine facies (#29, #17, Table 1) (Fig. 8).

The lowermost constraint on minimum RSL lowering for the early Holocene (7730±160 ^{14}C a BP, 8560 $^{+440}_{-350}$ cal. a BP) comes from the Kaslutt site, north of Richards Island, where a sandy fibrous peat sample containing fungal spores but barren of palynomorphs, indicated deposition above mean sea level (#16, Table 1, Fig. 8) (Hill *et al.* 1993). A date of 6000±70 ^{14}C a BP (6840 $^{+300}_{-170}$ cal. a BP) provides a constraint on minimum sea-level lowering from the easterly positioned North Tingmiark (NT-82-SO1) borehole (#8, Table 1, Fig. 8). It was obtained from the top of a 50 m thick sandy sequence underlying a few centimeters of seafloor clay (Hill *et al.* 1985). Palynological data from the sandy sequence showed a progression from fluvial through freshwater pond to ephemeral delta pond (with minor marine microplankton) environments (Hill *et al.* 1985). The radiocarbon date was obtained from an organic rich peaty clay sample containing wood and moss macrofossils, as well as abundant pollen and spores (Hill *et al.* 1985). Another freshwater peat sample was dated from the Isserk Borehole (BH6, #3, Table 1, Fig. 8) providing a late Holocene (3740±70 ^{14}C a BP, 4100 $^{+280}_{-210}$ cal. a BP) minimum-limiting constraint for RSL. The peat sample was also taken from the top of a sandy sequence, and contained large pieces of structureless terrestrial plant material, pollen, amorphous charcoal and filamentous root tissue (Hill *et al.* 1985). The lithology, palynology and presence of well-preserved rootlets, suggest a floodplain environment inhabited by grasses and sedge (Hill *et al.* 1985).

Prior to this study, the oldest radiocarbon age constraining the magnitude of Holocene transgression was from an unidentified marine bivalve (3970±120 ^{14}C a BP, 3570 $^{+350}_{-390}$ cal. a BP), collected from foraminifera-bearing silty clay landward of the MTW01 borehole on the Yukon coastal plain (#29, Table 1, Fig. 8) (Hill *et al.* 1993).

As this unidentified mollusc may have been a deposit-feeder, the validity of this RSL index point could be questioned due to the possible influence of the *Portlandia* effect (England *et al.* 2013). Similarly the two youngest marine samples from Table 1 constraining late Holocene RSL are both from collections of mollusc fragments that contain *Portlandia frigida* and *Portlandia arctica* (#18 and #19, Table 1, Fig. 8). Due to their detrital feeding habit, these species are no longer considered reliable for radiocarbon dating, and may significantly overestimate the true age of the sample (England *et al.* 2013).

The final existing constraint on maximum sea-level lowering comes from a large diameter (10 cm) piece of well-preserved wood (3530 ± 80 ^{14}C a BP, 3810^{+260}_{-200} cal. a BP) recovered from a marine deposit (foraminifer bearing silty clay) in the BH15+00 borehole, located north of Richards Island (#17, Table 1, Figs 1, 8) (Hill *et al.* 1993). We present no new data to further evaluate these constraints. In combination with the new data from MTW01, they provide the best field-based data for constraining middle Holocene RSL change on the Beaufort Sea Shelf.

The new early Holocene sea-level constraints from MTW01 agree with the RSL estimates provided by ICE6G_C(VM5a) for grid cells within the Mackenzie Trough region (Fig. 8) (Peltier *et al.* 2015). ICE6G_C is a model for global ice thickness changes from the Last Glacial Maximum to the present. It is coupled to a model of the Earth's rheological structure (VM5a) to predict regional isostatic adjustments due to changing ice mass distributions (Peltier *et al.* 2015). As such, sea-level predictions are dependent on accurate representations for the thickness and distribution of glacial ice.

In the vicinity of the Mackenzie Trough, (from the Yukon coastal plain to Richards Island, Fig. 8), ICE6G_C predicts maximum ice thicknesses at 26 cal. ka BP, with variable retreat rates resulting in the absence of land-based ice between 15.5 and 18.5 cal. ka BP (Fig. 8). Glacial isotatic adjustments result in sea-level variations along the inner shelf of >20 m, and a maximum sea-level lowstand following deglaciation of -112 to -117 m (Fig. 8). However, ICE6G_C further suggests that these regional variations in RSL were short-lived and dissipated quickly during the latest Pleistocene, resulting in similar rates and magnitudes of RSL change since ~12 cal. ka BP (Fig. 8). This is not the case over the eastern Tuktoyuktuk Peninsula, where ICE6G_C predicts thicker ice cover, which decreased in size but remained in place, until approximately the end of the Sitidgi Stade (Fig. 8). The impact on RSL was a shallower maximum lowstand, and slightly lower RSL during the early and middle Holocene in grid cells that cover the modern shoreline (Fig. 8). Further offshore (grid cells J and K, Fig. 8), maximum sea-level lowering was dramatically reduced, and a higher RSL is found through the early and middle Holocene. These observations are important as they highlight potential regional variability in RSL. τ

It is also important to note that ICE6G_C predicts the retreat of glacial ice from the grid cell occupied by MTW01 by 17 cal. ka BP, which is not in agreement with the proposed arrival of ice on Hershel Island after 16.2 ± 0.6 cal. ka BP (Fritz *et al.* 2012). Therefore, while the new RSL constraints from MTW01 fortuitously fit with estimates from ICE6G_C(VM5a) at 9-10 cal. ka BP, the magnitude and timing of the deglacial RSL lowstand remains unclear, which further renders uncertain rates of RSL change during the early and middle Holocene (Fig. 8). While knowledge of the RSL lowstand is incomplete, the new early Holocene RSL constraints limit the timing

of the postglacial RSL lowstand to prior to ~9.5 cal ka BP. The new constraint for early Holocene RSL from this study can be used in future modelling efforts to resolve the extent and timing of glacial ice in this sector of the Beaufort Sea during the late Wisconsinan. Due to the notably large predicted variability in RSL due to glacioisostatic adjustments, this should be done in conjunction with a glacioisostatic model. Furthermore, such efforts would benefit from more closely-spaced RSL index points, which could potentially be obtained from foraminifera-bearing marine sediments in other legacy boreholes that were not possible to date at the time drilling.

Timing of delta progradation

Hill (1996) initially assigned the progradational phase (Units E-C) to the Sitidgi Stade, which he correctly argued was a likely re-advance of the retreating Late Wisconsinan ice sheet. Their arguments for this were i) the re-advancing ice sheet would provide the sediment supply needed for the construction of a large subaerial delta, ii) the landward thinning of the progradational sequence was consistent with a sediment source close to the Sitidgi Stade limits, and iii) the deltaic nature of the parasequence was not consistent with subglacial emplacement while a thick ice stream occupied the Mackenzie Trough (*i.e.* during the Toker Point Stade) (Hill *et al.* 1996). The age assignment was consistent with the palynological data, reportedly indicating deposition since approximately 14 cal. ka BP (Blasco *et al.* 1990), although the abundance of reworked palynomorphs makes this age assignment weakly constrained.

The absence of marine calcareous biogenic material in Units C through E precludes any absolute age assignment to the progradational phase. The ^{14}C ages from

the $\text{POC}_{>63\mu\text{m}}$ do provide maximum-limiting ages for deposition that help constrain the relative timing. The youngest age, obtained from the base of the sequence, indicates that progradation occurred after $24\,820^{+390}_{-380}$ cal. a BP (Table 3, Fig. 6). Strictly speaking this age pre-dates the arrival of Toker Point ice along the Tuktoyaktuk Peninsula (22-16 cal. ka BP) (Murton *et al.* 2010). However, the true age of progradation is certainly younger than this, as the carbon in these samples was eroded and transported offshore by the proglacial-Mackenzie River. This is reflected by the low $\delta^{13}\text{C}$ values (-26.0‰ to -26.8‰) which are similar to the modern day Mackenzie River (Goni *et al.* 2005; Hilton *et al.* 2015), indicating a dominantly terrigenous source for the organic matter (Fig. 4), and the large measured offsets between paired samples in Unit A.

In the modern Mackenzie River suspended particulate matter (SPM) is composed of a mixture of modern-higher plant derived material and older material from eroded peatlands, permafrost, and rock-derived material (Hilton *et al.* 2015; Vonk *et al.* 2016). River depth profile samples of SPM collected from the main stem of the Mackenzie River in the delta in 2010 and 2011 provide constraints on the modern-day ^{14}C age of POC across a range of suspended load grain sizes (Hilton *et al.* 2015). These samples range in age of 4548 ± 38 to 9480 ± 42 ^{14}C a BP, with an average ^{14}C age of 7563 ± 1420 a BP ($n = 8$, \pm standard deviation) (Hilton *et al.* 2015). The most ^{14}C -depleted POC are found near the surface of the river (0-6 m water depth) associated with the finest clastic sediment. Based on nitrogen to organic carbon ratios, it is thought that vegetation and aged soil-derived material makes up ~70-80% of this material, and rock-derived POC the remainder (Hilton *et al.* 2015).

While the variability in the modern river system is large, the bulk POC has a similar ^{14}C age as the average offset (8400 ± 850 ^{14}C a) found in this study between the $\text{POC}_{>63\mu\text{m}}$ ages and the paired measurements on either benthic foraminifera or mollusc fragment samples in Unit A (Figs. 6, 7). It is not known whether this average offset applies to the lower units (C-E) in the borehole where calcareous micro- and macrofossils are absent. Differences in the proportion of rock-derived organic carbon, and/or changes in the residence time of organic matter in soils of the Mackenzie Basin over time (MacDonald *et al.* 2006) would cause this offset to vary. We suggest that it provides a minimum estimate for the offset between the radiocarbon age of terrestrial organic carbon collected from units C–E and the true depositional age. As previously stated, we assume that Units C–E contain larger proportions of re-deposited terrestrial organic carbon and less organic carbon derived from contemporaneous marine productivity. If 8400 ± 850 ^{14}C years is subtracted from the youngest age of the progradational facies ($20\,600 \pm 118$ ^{14}C a BP, 43B, Table 3) a date of $12\,200 \pm 970$ ^{14}C ka BP is found, equivalent to 15.3–10.3 cal. ka BP (2σ). This is clearly not a robust absolute age constraint on deposition, but combined with the overlapping ^{14}C ages from $\text{POC}_{>63\mu\text{m}}$ in Units C–E (samples 43B to 24B) do suggest that all these units were deposited during deglaciation, as suggested by Blasco *et al.* (1990), after Toker Point ice had retreated from the coast (Hill, 1996) (Fig. 6).

Meltwater events

Along the Tuktoyaktuk Peninsula and on Richards Island, the retreat of glacial ice was followed by aeolian dune building and sand sheet aggradation (Rampton 1988; Dallimore *et al.* 1997; Murton *et al.* 1997; Bateman & Murton, 2006; Murton *et al.* 2007, 2010). Deposition of this postglacial sand above Toker Point till was

interrupted by periods of fluvial erosion attributed to glacial meltwater outburst floods (Murton *et al.* 2010). Two episodes of fluvial erosion are identified based on OSL dating of interbedded aeolian sands (Murton *et al.* 2010). The first occurred between 13.0±.2 cal. ka BP and 11.7±0.1 cal. ka BP and possibly during the Younger Dryas, while the second occurred between 11.7±0.1 cal. ka BP and 9.3±0.7 cal. ka BP (Murton *et al.* 2010).

Murton *et al.* (2010) further suggested that the unconformity separating units C and B in MTW01 may have developed as a response to the earlier episode of fluvial erosion (i.e. prior to marine transgression) during a Younger Dryas outburst flood. The lack of dateable material at the base of Unit B prevents us from directly testing this hypothesis. For example, if a Younger Dryas or older age had been returned from sediments in Unit B (i.e following transgression at the site), we would have been able to reject the hypothesis of Murton *et al.* (2010) that the Unit C-B transition was first formed during a glacial meltwater outburst, and later reworked during transgression.

The new radiocarbon dates simply indicate that this remains a tenable hypothesis that requires further testing. This can be shown in 2 ways. Extrapolating the linear sedimentation rate of 2.65±0.06 m ka⁻¹ from the top of Unit B (9400⁺¹⁸⁰₋₂₆₀ cal. a BP) at ~22 m b.s.f. (sample 15B, Table 2) to the Unit B/C transition at 29 m b.s.f., the estimated age of the boundary (11.8–12.2 cal. ka BP) falls within the Younger Dryas. Similarly, subtracting the 8400±850 ¹⁴C year offset from the POC_{>63 μ} date near the base of Unit B (18 595±100 ¹⁴C a BP, 21B, Table 3) results in an age of 10 195±950 ¹⁴C ka BP, equivalent to 14.0-9.2 cal. ka BP (2σ), which again brackets the Younger Dryas. As with the estimate for the maximum age of progradation, this

is not an absolute date, but illustrates that a Younger Dryas age for the Unit B/C transition remains tenable, given the existing constraints. However, this would imply a much higher RSL during the Younger Dryas than is currently modelled by ICE6G_C(VM5a) (Fig. 8).

In MTW01, the transition between Units B and A (8660^{+300}_{-260} cal. a BP) overlaps with the second episode of fluvial erosion identified on Richards Island (9300 ± 700 cal. a BP) by Murton *et al.* (2010). However, this may simply be a coincidence, as the marine character of Unit B, its slightly coarser composition than the overlying Unit A sediments, and its correlation to the sigmoidally shaped offshore healing phase wedge (Fig. 3; Moran *et al.* 1989) all indicate that the large scale stratal architecture was formed in response to marine transgression (Posamentier & Allen 1993).

In seismic data, the transition between Units B and A is disconformable at the drilling site, and becomes conformable further offshore (Moran *et al.* 1989). Although its exact duration is difficult to resolve, this disconformity is related to a relatively short hiatus (Figs 6, 7). The median calibrated ages are offset by 740 years, but considering the 2σ uncertainty, the true offset could be anywhere between 180 or 1180 years.

Conclusions

This study aimed to better constrain the absolute chronology of the 81.5 m deep MTW01 borehole using radiocarbon dating. Specifically, it set out to date a period of delta progradation prior to postglacial transgression of the site, identify Younger Dryas-aged strata, and constrain postglacial RSL change. A lack of dateable organic

carbon below 22 m b.s.f. precluded addressing the first two objectives directly.

Nonetheless, we can conclude that:

- Based on dating of particulate organic carbon in the $>63 \mu\text{m}$ size fraction, the progradational parasequence accumulated rapidly sometime after $24\,820^{+390}_{-380}$ cal. a BP. Accounting for modern and Holocene offsets in the POC ages, it is likely that this phase of progradation occurred following ice sheet retreat from the Toker Point Stade limit dated between ~ 22 and 16 cal. ka BP on the Tuktoyaktuk peninsula and Richards Island by Murton et al (2007).
- Based on a radiocarbon date from a sample of marine mollusc fragments, transgression at this site occurred before 9400^{+180}_{-260} cal. a BP. The new early Holocene RSL constraints indicate that the postglacial RSL lowstand occurred prior to ~ 9.5 cal. ka BP.
- Although this constraint on early Holocene RSL agrees well with predictions from ICE6G_C(VM5a) for this location of the Beaufort Sea, additional data are needed to constrain the timing and magnitude of the RSL lowstand prior to ~ 9.5 cal. ka BP.
- The absence of material capable of providing absolute dates below 22 m b.s.f., prevents the identification of the stratigraphic interval associated with the Younger Dryas and precludes a test of whether a glacial outburst flood eroded the top of the progradational sequence (Unit C) prior to marine inundation. Our results only suggest that this remains a tenable hypothesis.
- Holocene deposition of the overlying foram-bearing marine clay of Unit A occurred at a linear sedimentation rate of $2.65 \pm 0.06 \text{ m ka}^{-1}$. Similar to other sediment cores from the Mackenzie Trough, Holocene sediments contain

relatively abundant numbers of planktic and benthic microfossils and therefore make them potentially valuable high-resolution palaeoceanographic archives.

Acknowledgements

We would like to thank the editor and 2 anonymous reviewers who provided exceptionally helpful and thorough reviews of the manuscript. Radiocarbon measurements on foraminifera and mollusc fragments were funded by the Swedish Research Council (VR) grants to M. O'Regan and H. Coxall. Radiocarbon measurements on the particulate organic matter were funded by the Natural Environment Research Council (NERC), UK (Allocation 1611.0312) to R.G. Hilton and an Early Career Research Grant by the British Society for Geomorphology.

Figure and Table Captions

Table 1. Terrestrial and marine samples from the Beaufort Sea used to constrain Holocene RSL change. Original ^{14}C dates from Hill *et al.* (1985, 1993) were calibrated using either the Marine13 calibration curve and a ΔR of 335 ± 85 years or the IntCal13 dataset for terrestrial organic materials (Reimer *et al.* 2013). All calibrated ages are rounded to the nearest decade, and reported with the 95.4% (2σ) confidence interval. Locations of sites are shown in Figs 1 and 8. Asterisks beside site numbers indicate marine samples that did, or may have, contained deposit-feeding molluscs susceptible to having exaggerated radiocarbon ages.

Table 2. Radiocarbon measurements on benthic foraminifera (BF) and mollusc fragment (MF) samples from MTW01. All samples were measured at the National Ocean Sciences AMS Facility (NOSAMS), Woods Hole Oceanographic Institution.

Ages were calibrated using the Marine13 calibration curve (Reimer *et al.* 2013) and a ΔR of 335 ± 85 years (Coulthard *et al.* 2010).

Table 3. Radiocarbon measurements from MTW01 on particulate organic matter collected from the $>63 \mu\text{m}$ sample fractions. All ages were calibrated using the IntCal13 calibration curve (Reimer *et al.* 2013).

Figure 1. Study area in the Canadian Beaufort Sea with limits of the Toker Point/Buckland glaciation (blue) and Sitidgi Stade (red) drawn after Rampton (1988) and Hughes (1987) respectively. Bathymetry and modern shorelines are from IBCAO_V3 (Jakobsson *et al.* 2012). Location of the MTW01 borehole is shown (yellow) along with location of radiocarbon ages (white dots) used to construct a regional Holocene sea-level curve for the Beaufort Sea by Hill *et al.* (1985, 1993).

Figure 2. Global ice equivalent sea level (Lambeck *et al.* 2014) compared with the RSL curve for the Beaufort Shelf proposed by Hill *et al.* (1985, 1993) (blue line). Sea-level index points are from offshore boreholes (Fig. 1, Table 1) compiled by Hill *et al.* (1985, 1993) and calibrated in this study (see Table 1 for details). Calibrated age uncertainty (2σ) shown by horizontal bars. Black triangles are maximum RSL index points, and white triangles minimum RSL index points, depending on the type and stratigraphic nature of material that was dated (Table 1) (Hill *et al.* 1985, 1993). The maximum sea-level lowstand of -70 m was inferred by Hill *et al.* (1985, 1993) by the observed depth to incised valleys on the Beaufort shelf.

Figure 3. Interpreted stratigraphy of the Mackenzie Delta and upper Trough. Image redrawn from interpreted seismic profiles (Hill 1996). Location of the MTW01 borehole is shown in close proximity to the hinge line defining the seaward edge of the progradational sequence. Healing phase deposits, following marine transgression, thicken seaward of the hinge line. The stratigraphy and depositional interpretation of the MTW01 borehole is redrawn from Moran *et al.* (1989). Seaward from the borehole, a sediment wedge originally described as a healing phase deposit separates the uppermost clinoform of the progradational parasequence and the seaward extension of the marine inundation surface (Hill 1996).

Figure 4. Grain size, TOC, $\delta^{13}\text{C}$ of the $\text{POC}_{>63\mu\text{m}}$ and abundance of biogenic material identified in the $>63\mu\text{m}$ size fraction. Counting results are presented as the number of specimens (or fragments) per dry gram of the total sample. Raw count numbers are provided in Table S1.

Figure 5. Photomicrographs of mollusc shell fragments from sample 16B (21.64–22.00 m b.s.f.). Yellowish-brown coating on the fragments is remains of the periostracum.

Figure 6. A. Stratigraphy of MTW01 (Moran *et al.* 1989) and calibrated age ranges (2σ) for the $\text{POC}_{>63\mu\text{m}}$ (green), benthic foram (red) and mollusc fragment samples (blue). Horizontal dashed lines represent depth uncertainty of the samples based on sample thickness. Arrows mark position of cited biostratigraphic pollen-based dates presented by Blasco *et al.* (1990). Age range for the Younger Dryas, Sitidgi Stade and Toker Point/Buckland glaciation are given and correspond to reported dates in the

text. A linear interpolation model performed in CLAM (Blaauw, 2010) was applied to all foraminifera and mollusc fragment samples from Unit A. Results are shown by the black solid line with the 95% confidence band shaded grey. Modelled age for each sample is given in Table 2. The modelled ages were used to estimate a linear sedimentation rate of 2.65 ± 0.06 m ka⁻¹ for Unit A sediments in MTW01.

Figure 7. Comparison of uncalibrated ¹⁴C ages of the POC_{>63μm} with uncalibrated ¹⁴C measurements on either paired benthic foram (circles) or mollusc fragment (squares). The average and standard deviation (8400 ± 850 ¹⁴C a BP) of the difference between these measurements is shown by the grey bar and black line. Numbers above the sample symbols are the δ¹³C (‰) of the POC_{>63μm}. Modern-day particulate organic matter in the suspended load of the Mackenzie River, with an age of 7563 ± 1420 ¹⁴C a BP (n = 8, ± standard deviation) (Hilton *et al.* 2015).

Figure 8. Comparison of model estimates of RSL and offshore constraints from the Beaufort Sea. **A.** Location of grid cells from which ice thickness and sea level are extracted from ICE6G_C(VM5a) (Peltier *et al.* 2015). Also shown are locations for MTW01 and radiocarbon-dated RSL constraints from Table 1. **B.** Age and modelled ice thickness from ICE6G in grid cells shown in panel (A). Age range for the Younger Dryas (YD), Sitidgi Stade and Toker Point/Buckland glaciation are given and correspond to reported dates in the text. The period encompassing reported episodes of fluvial erosion on Richards Island is from Murton *et al.* (2010). **C.** New RSL constraints from this study (open triangles) and previously published RSL constraints (shaded triangles) from the Beaufort Sea (Table 1; Hill *et al.* 1993) compared to RSL estimates from ICE6G_C(VM5a) along the same transect of grid

cells as in panel (A). Constraints on maximum RSL are shown as triangles, while minimum constraints on RSL are inverted triangles. Variation in predicted RSL from ICE6G_C is highlighted by shading, with heavier shading applied to the area encompassed by grid cells A-E (panel A), where postglacial RSL is relatively consistent. Global ice equivalent sea level (Lambeck *et al.* 2014) is shown by the grey line and error bars, and the existing field-based curve for the Beaufort shelf from Hill *et al.* (1993) as solid and dashed blue lines. Numbers on sea-level index points refer to data labels in Fig. 1 and Table 1 that are specifically discussed in the text.

Supporting information

Table S1. Micro- and macrofossil content of samples from the MTW01 borehole.

Figure S1. Photomicrographs of representative benthic foraminifers from MTW01 samples 15B, 12B and 4A. A-C: *Elphidium excavatum subsp. clavatum*, D-E: *Cassidulina reniformis*, G-I: *Bolivina arctica*, J-K: *Cassidulina teretis*. Scale bars are all 200 μm , except for J, which is 500 μm . Images were taken using a Leica M205 C microscope with camera system.

References

- Andrews, J. T. & Dunhill, G. 2004: Early to mid-Holocene Atlantic influx and deglacial meltwater events, Beaufort Sea Slope, Arctic Ocean. *Quaternary Research* 61, 14-21.
- Batchelor, C. L., Dowdeswell, J. A., & Pietras, J. T. 2013a: Seismic stratigraphy, sedimentary architecture and palaeo-glaciology of the Mackenzie Trough: evidence for two Quaternary ice advances and limited fan development on the western Canadian Beaufort Sea margin. *Quaternary Science Reviews* 65, 73-87.
- Batchelor, C. L., Dowdeswell, J. A., & Pietras, J. T. 2013b: Variable history of Quaternary ice-sheet advance across the Beaufort Sea margin, Arctic Ocean. *Geology* 41, 131-134.

- 796 Bateman, M. D. & Murton, J. B. 2006: Late Pleistocene glacial and periglacial aeolian
797 activity in the Tuktoyaktuk Coastlands, NWT, Canada. *Quaternary Science Reviews*
798 25, 2552–2568.
- 799 Beget, J. 1987: Low profile of the northwest Laurentide Ice Sheet. *Arctic and Alpine*
800 *Research* 19, 81–88.
- 801 Blaauw, M. 2010: Methods and code for ‘classical’ age-modelling of radiocarbon
802 sequences. *Quaternary Geochronology* 5, 512–518.
- 803 Bostok, H. S. 1948: Physiography of the Canadian Cordillera, with special reference
804 to the area north of the fifty-fifth parallel. *Geological Survey of Canada, Memoir*
805 247, 106 pp.
- 806 Blair, N. E., Leithold, E. L., Ford, S. T., Peeler, K. A., Holmes, J. C. & Perkey, D. W.
807 2003: The persistence of memory: The fate of ancient sedimentary organic carbon
808 in a modern sedimentary system. *Geochimica et Cosmochimica Acta* 67, 63–73,.
- 809 Blasco, S. M., Fortin, G., Hill, P. R., O’Connor, M. J. & Brigham-Grette, J. 1990: The
810 late Neogene and Quaternary stratigraphy of the Canadian Beaufort continental
811 shelf. In Grantz, A., Johnson, L. & Sweeney, J. F. (eds.): *The Geology of North*
812 *America. The Arctic Ocean Region, vol. L*, 491–502. Geological Society of
813 America, Boulder.
- 814 Blasco, S., Bennett, R., Brent, T., Burton, M., Campbell, P., Carr, E., Covill, R.,
815 Dallimore, S., Davies, E., Hughes-Clarke, J., Issler, D., MacKillop, K., Mazzotti,
816 S., Patton, E., Shearer, J. & White, M. 2011: 2010 State of knowledge: Beaufort
817 Sea seabed geohazards associated with offshore hydrocarbon development.
818 *Geological Survey of Canada, Open File* 6989, 335 pp.
- 819 Bringue, M. & Rochon, A. 2012: Late Holocene paleoceanography and climate
820 variability over the Mackenzie Slope (Beaufort Sea, Canadian Arctic). *Marine*
821 *Geology* 291, 83–96.
- 822 Coulthard, R. D., Furze, M. F. A., Pienkowski, A. J., Nixon, F. C. & England, J. H.
823 2010: New marine ΔR values for Arctic Canada. *Quaternary Geochronology* 5,
824 419–434.
- 825 Condron, A. & Winsor, P. 2012: Meltwater routing and the Younger Dryas.
826 *Proceedings of the National Academy of Sciences* 109, 19928–19933.
- 827 Dallimore, S. R., Wolfe, S. A., Matthews, J. V. Jr. & Vincent, J-S. 1997: Mid-
828 Wisconsinan eolian deposits of the Kittigazuit Formation, Tuktoyaktuk Coastlands,

- 829 Northwest Territories, Canada. *Canadian Journal of Earth Sciences* 34, 1421–
830 1441.
- 831 Dyke, A. S. & Prest, V. K. 1987: The Late Wisconsinan and Holocene history of the
832 Laurentide Ice Sheet. *Géographie physique et Quaternaire* 41, 237–263.
- 833 Dyke, A. S., Andrews, J. T., Clark, P. U., England, J. H., Miller, G. H., Shaw, J. &
834 Veillette, J. J. 2002: The Laurentide and Innuitian ice sheets during the Last Glacial
835 maximum. *Quaternary Science Reviews*, 21, 9–31.
- 836 Dyke, A. S. 2004: An outline of the deglaciation of North America with emphasis on
837 central and northern Canada. In Ehlers, J. & Gibbard, P. L. (eds.): *Quaternary*
838 *Glaciations, Extent and Chronology. Part II. North America. Developments in*
839 *Quaternary Science* 2B, 371–406. Elsevier, Amsterdam.
- 840 England, J. H., Furze, M. F. A. & Doupé, J. P. 2009: Revision of the NW Laurentide
841 Ice Sheet: implications for paleoclimate, the northeast extremity of Beringia, and
842 Arctic Ocean sedimentation. *Quaternary Science Reviews* 28, 1573–1596.
- 843 England, J., Dyke, A.S., Coulthard, R.D., McNeely, R. & Aitken, A. 2013: The
844 exaggerated radiocarbon age of deposit-feeding molluscs in calcareous
845 environments. *Boreas* 42, 362–373.
- 846 Fritz, M., Wetterich, S., Schirrmesidter, L., Meyer, H., Lantuit, H., Preusser, F. &
847 Pollard, W. H., 2012: Eastern Beringia and beyond: Late Wisconsinan and
848 Holocene landscape dynamics along the Yukon Coastal Plain, Canada.
849 *Palaeogeography, Palaeoclimatology, Palaeoecology* 319–320, 28–45.
- 850 Galy, V., Beyssac, O., France-Lanord, C. & Eglinton T. 2008: Recycling of graphite
851 during Himalayan erosion: A geological stabilization of carbon in the crust.
852 *Science* 322, 943–945.
- 853 Goñi, M. A., Yunker, M. B., Macdonald, R. W. & Eglinton, T. I. 2005: The supply
854 and preservation of ancient and modern components of organic carbon in the
855 Canadian Beaufort Shelf of the Arctic Ocean. *Marine Chemistry* 93, 53–73.
- 856 Goñi, M. A., O'Connor, A., Kuzyk, Z. Z., Yunker, M. & Gobeil, C. 2013:
857 Distribution and sources of organic matter in surface marine sediments across the
858 North American Arctic margin. *Journal of Geophysical Research - Oceans* 118,
859 4017–4035.
- 860 Heier-Nielsen, S., Conradsen, K., Heinemeier, J., Knudsen, K. L., Nielsen, H., Rud,
861 N. & Sveinbjörnsdóttir, Á. E. 1995: Radiocarbon Dating of Shells and

- 862 Foraminifera from the Skagen Core, Denmark: Evidence of Reworking.
863 *Radiocarbon* 37, 119-130.
- 864 Hill, P. R., Mudie, P. J., Moran, K. & Blasco, S.M. 1985: A sealevel curve for the
865 Canadian Beaufort Shelf. *Canadian Journal of Earth Sciences* 22, 1383–1393.
- 866 Hill, P. R., Héquette, A. & Ruz, M.-H. 1993: Holocene sea-level history of the
867 Canadian Beaufort Shelf. *Canadian Journal of Earth Sciences* 30, 103–108.
- 868 Hill, P. R., 1996. Late Quaternary sequence stratigraphy of the Mackenzie Delta.
869 *Canadian Journal of Earth Sciences* 33, 1064-1074.
- 870 Hilton, R. G., Galy, V., Gaillardet J., Dellinger, M., Bryant, C., O'Regan, M., Gröcke,
871 D. R., Coxall, H., Bouchez, J. & Calmels, D. 2015: Erosion of organic carbon in
872 the Arctic as a geological carbon dioxide sink. *Nature* 524, 84-87.
- 873 Hilton, R. G. and Galy, A., Hovius, N., Horng, M.-J. & Chen, H. 2010: The isotopic
874 composition of particulate organic carbon in mountain rivers of Taiwan,
875 *Geochimica et Cosmochimica Acta* 74, 3164-3181.
- 876 Hughes, O. L. 1987: Late Wisconsinan Laurentide glacial limits of northwestern
877 Canada: the Tutsieta Lake and Kelly Lake phases. *Geological Survey of Canada*,
878 *Paper* 85-25, 19 pp.
- 879 Jakobsson, M., Mayer, L. A., Coakley, B., Dowdeswell, J. A., Forbes, S., Fridman,
880 B., Hodnesdal, H., Noormets, R., Pedersen, R., Rebesco, M., Schenke, H.-W.,
881 Zarayskaya, Y. Accettella, D., Armstrong, A., Anderson, R. M., Bienhoff, P.,
882 Camerlenghi, A., Church, I., Edwards, M., Gardner, J. V., Hall, J. K., Hell, B.,
883 Hestvik, O. B., Kristoffersen, Y., Marcussen, C., Mohammad, R., Mosher, D.,
884 Nghiem, S. V., Pedrosa, M. T., Travaglini, P. G. & Weatherall, P. 2012: The
885 International Bathymetric Chart of the Arctic Ocean (IBCAO) Version 3.0,
886 *Geophysical Research Letters* 39, L12609. 6 pp.
- 887 Jakobsson, M., Andreassen, K., Bjarnadóttir, L. R., Dove, D., Dowdeswell, J. A.,
888 England, J. H., Funder, S., Hogan, K., Ingólfsson, Ó., Jennings, A., Larsen, N. K.,
889 Kirchner, N., Landvik, J. Y., Mayer, L., Mikkelsen, N., Möller, P., Niessen, F.,
890 Nilsson, J., O'Regan, M., Polyak, L., Nørgaard-Pedersen, N., & Stein, R. 2014:
891 Arctic Ocean glacial history. *Quaternary Science Reviews* 92, 40-67.
- 892 Kao, S.-J., Hilton, R., Selvaraj, K., Dai, M., Zehetner, F., Huang, J.-C., Hsu, S.-C.,
893 Sparkes, R., Liu, J. & Lee, T.-Y. 2014: Preservation of terrestrial organic carbon

- 894 in marine sediments offshore Taiwan: Mountain building and atmospheric carbon
895 dioxide sequestration. *Earth Surface Dynamics* 2, 127–139.
- 896 Komada, T., Anderson, M. R. & Dorfmeier, C. L. 2008: Carbonate removal from
897 coastal sediments for the determination of organic carbon and its isotopic
898 signatures, ^{13}C and ^{14}C : Comparison of fumigation and direct acidification by
899 hydrochloric acid. *Limnology and Oceanography* 6, 254–262.
- 900 Lacelle, D., Lauriol, B., Zazula, G., Chaleb, B., Utting, N. & Clark, I. D. 2013:
901 Timing of advance and basal condition of the Laurentide Ice Sheet during the last
902 glacial maximum in the Richardson Mountains, NWT. *Quaternary Research* 80,
903 274–283.
- 904 Lakeman, T. R. & England, J. H. 2012: Paleoglaciological insights from the age and
905 morphology of the Jesse moraine belt, western Canadian Arctic. *Quaternary*
906 *Science Reviews* 47, 82–100.
- 907 Lakeman, T. R. & England, J. H. 2013: Late Wisconsinan glaciation and postglacial
908 relative sea-level change on western Banks Island, Canadian Arctic Archipelago.
909 *Quaternary Research* 80, 99–112.
- 910 Lambeck, K., Rouby, H., Purcel, A., Sun, Y. & Sambridge, M. 2014: Sea level and
911 global ice volumes from the Last Glacial Maximum to the Holocene. *Proceedings*
912 *of the National Academy of Sciences* 111, 15296–15303.
- 913 Macdonald, R. W., Solomon, S. M., Cranston, R. E., Welch, H. E., Yunker, M. B. &
914 Gobeil, C. 1998: A sediment and organic carbon budget for the Canadian Beaufort
915 Shelf. *Marine Geology* 144, 255–273.
- 916 MacDonald, G. M., Beilman, D. W., Kremenetski, K. V., Sheng, Y., Smith, L. C. &
917 Velichko, A. A. 2006: Rapid development of the circumarctic peatland complex
918 and atmospheric CH_4 and CO_2 variations. *Science* 314, 285–288.
- 919 Mackay, J. R., Rampton, V. N. & Fyles, J. G. 1972: Relic Pleistocene permafrost,
920 western Arctic Canada. *Science* 176, 1321–1323.
- 921 McClelland, J. W., Homes, R. M., Peterson, B. J., Raymond, P. A., Striegl, R. G.,
922 Zhulidov, A. V., Zimov, S. A., Zimov, N., Tank, S. E., Spencer, R. G. M., Staples,
923 R., Gurtovaya, T. Y. & Griffin, C. G. 2016: Particulate organic carbon and
924 nitrogen export from major Arctic rivers. *Global Biogeochemical Cycles* 30. 629–
925 643.

- 926 Mekik, F. 2014: Radiocarbon dating of planktonic foraminifer shells: A cautionary
927 tale. *Paleoceanography* 29, 13-29.
- 928 Moran, K., Hill, P. R. & Blasco, S. M. 1989: Interpretation of piezocone penetrometer
929 profiles in sediment from the Mackenzie Trough, Canadian Beaufort Sea. *Journal*
930 *of Sedimentary Petrology* 59, 88 - 97.
- 931 Murton, J. B., Bateman, M. D., Dallimore, S. R., Teller, J. T. & Yang, Z. 2010:
932 Identification of Younger Dryas outburst flood path from Lake Agassiz to the
933 Arctic Ocean. *Nature* 464, 740-743.
- 934 Murton, J. B., Frechen, M. & Maddy, D. 2007: Luminescence dating of mid- to Late
935 Wisconsinan aeolian sand as a constraint on the last advance of the Laurentide Ice
936 Sheet across the Tuktoyaktuk Coastlands, western Arctic Canada. *Canadian*
937 *Journal of Earth Sciences* 44, 857-869.
- 938 Murton, J. B., French, H. M. & Lamothe, M. 1997: Late Wisconsinan erosion and
939 eolian deposition, Summer Island area, Pleistocene Mackenzie Delta, Northwest
940 Territories: optical dating and implications for glacial chronology. *Canadian*
941 *Journal of Earth Sciences* 34, 190–199.
- 942 O'Connor, M. J. 1989: Surficial Geology of the Mackenzie Trough. *Geological*
943 *Survey of Canada, Open File Report*, 188 pp.
- 944 Peltier, W. R., Argus, D. F. & Drummond, R. 2015: Space geodesy constrains ice age
945 terminal deglaciation: The global ICE-6G_C (VM5a) model. *Journal of*
946 *Geophysical Research - Solid Earth* 120, 450–487.
- 947 Peltier, W. R., Vettoretti, G., & Stastna, M. 2006: Atlantic meridional overturning and
948 climate response to Arctic Ocean freshening. *Geophysical Research Letters* 33,
949 L06713.
- 950 Posamentier, H. W. & Allen, G.P. 1993: Variability of the sequence stratigraphic
951 model: effects of local basin factors. *Sedimentary Geology* 86, 91–109.
- 952 Rampton, V. N. 1982: Quaternary geology of the Yukon Coastal Plain. *Geological*
953 *Survey of Canada, Bulletin* 317, 49 pp.
- 954 Rampton, V. N. 1988: Quaternary geology of the Tuktoyaktuk Coastlands, Northwest
955 Territories. *Geological Survey of Canada, Memoir* 423, 98 pp.
- 956 Rasmussen, S. O., Andersen, K. K., Svensson, A. M., Steffensen, J. P., Vinther, B.
957 M., Clausen, H. B., Siggaard-Andersen, M-L., Johnsen, S. J., Larsen, L. B., Dahl-
958 Jensen, D., Bigler, M., Röthlisberger, R., Fishcer, H., Goto-Azuma, K., Hansson,

- 959 M. E. & Ruth, U. 2006: A new Greenland ice core chronology for the last glacial
960 termination. *Journal of Geophysical Research - Atmospheres* 111, D06102, 15pp.
- 961 Reimer, P. J., Bard, E., Bayliss, A., Beck, J. W., Blackwell, P. G., Bronk Ramsey, C.,
962 Buck, C. E., Cheng, H., Edwards, R. L., Friedrich, M., Grootes, P. M., Guilderson,
963 T. P., Hafliðsson, H., Hajdas, I., Hatté, C., Heaton, T. J., Hoffmann, D. L., Hogg,
964 A. G., Hughen, K. A., Kaiser, K. F., Kromer, B., Manning, S. W., Niu, M.,
965 Reimer, R. W., Richards, D. A., Scott, E. M., Southon, J. R., Staff, R. A., Turney,
966 C. S. M. & van der Plicht, J. 2013: IntCal13 AND Marine13 radiocarbon age
967 calibration curves 0–50,000 years cal BP. *Radiocarbon* 55, 1869-1887.
- 968 Shearer, J. M. 1971: Preliminary interpretation of shallow seismic reflection profiles
969 from the west side of Mackenzie Bay, Beaufort Sea. In: *Report of Activities, Part*
970 *B, Geological Survey of Canada, Paper 71-1*, 131-138.
- 971 Schell, T. M., Scott, D. B., Rochon, A. & Blasco, S. 2008: Late Quaternary
972 paleoceanography and paleo-sea ice conditions in the Mackenzie Trough and
973 Canyon, Beaufort Sea. *Canadian Journal of Earth Science* 45, 1399-1415.
- 974 Stokes, C. R., Clark, C. D. & Winsborrow, M. C. M. 2006: Subglacial bedform
975 evidence for a major palaeo-ice stream and its retreat phases in Amundsen Gulf,
976 Canadian Arctic Archipelago. *Journal of Quaternary Science* 21, 399–412.
- 977 Tarasov, L. & Peltier, W. R. 2005: Arctic freshwater forcing of the Younger Dryas
978 cold reversal. *Nature* 435, 662-665.
- 979 Taylor, A. E., Dallimore, S. R., Hill, P. R., Issler, D. R. Blasco, S. & Wright, F. 2013:
980 Numerical model of the geothermal regime on the Beaufort Shelf, arctic Canada
981 since the Last Interglacial. *Journal of Geophysical Research - Earth Surface* 118,
982 2365–2379.
- 983 Vincent, J-S. 1989: Quaternary geology of the northern Canadian Interior Plains. In
984 Fulton, R. J. (ed.): *Quaternary geology of Canada and Greenland. Geological*
985 *Survey of Canada, Geology of Canada*, 1, 100-137.
- 986 Vincent, J-S. 1992: The Sangamonian and early Wisconsinan glacial record in the
987 western Canadian Arctic. In Clark P. U. & Lea, P. D. (eds.): *The last interglacial-*
988 *glacial transition in North America*, 233-252. *Geological Society of America,*
989 *Special Paper 270*,.
- 990 Vincent, J.-S. & Prest, V.K. 1987. The Early Wisconsinan history of the Laurentide
991 Ice Sheet. *Géographie physique et Quaternaire* 41, 199-213.

- 992 Vonk, J. E., Dickens, A. F., Giosan, L., Hussain, Z. A., Kim, B., Zipper, S. C.,
993 Holmes, R. M., Montlucon, D. B., Galy, V. & Eglinton, T. I. 2016: Arctic Deltaic
994 Lake Sediments as recorders of fluvial organic matter deposition. *Frontiers of*
995 *Earth Science* 4:77, 24 pp.
- 996 Walker, M. J. C., Berkelhammer, M., Björck, S., Cwynar, L. C., Fisher, D. A., Long,
997 A. J., Lowe, J. J., Mewmha, R. M., Rasmussen, S. O. & Weiss, H. 2012: Formal
998 subdivision of the Holocene Series/Epoch: a Discussion Paper by a Working
999 Group of INTIMATE (Integration of ice-core, marine and terrestrial records) and
1000 the Subcommission on Quaternary Stratigraphy (International Commission on
1001 Stratigraphy). *Journal of Quaternary Science* 27, 649-659.
- 1002 Wegner, C., Bennett, K. E., de Vernal, A., Forwick, M., Fritz, M., Heikkilä, M.,
1003 Lacka, M., Lantuit, H., Laska, M., Moskalik, M., O'Regan, M., Pawłowska, J.,
1004 Promińska, A., Rachold, V., Vonk, J. E. & Werner, K. 2015: Variability in
1005 transport of terrigenous material on the shelves and the deep Arctic Ocean during
1006 the Holocene. *Polar Research* 34, 24964, 19 pp.
- 1007 Whiteside, J. H., Olsen, P. E., Eglinton, T. I., Cornet, B., McDonald, N. G. & Huber,
1008 P. 2011: Pangean great lake paleoecology on the cusp of the end-Triassic
1009 extinction. *Palaeogeography, Palaeoclimatology, Palaeoecology* 301, 1–17.

Table 1.

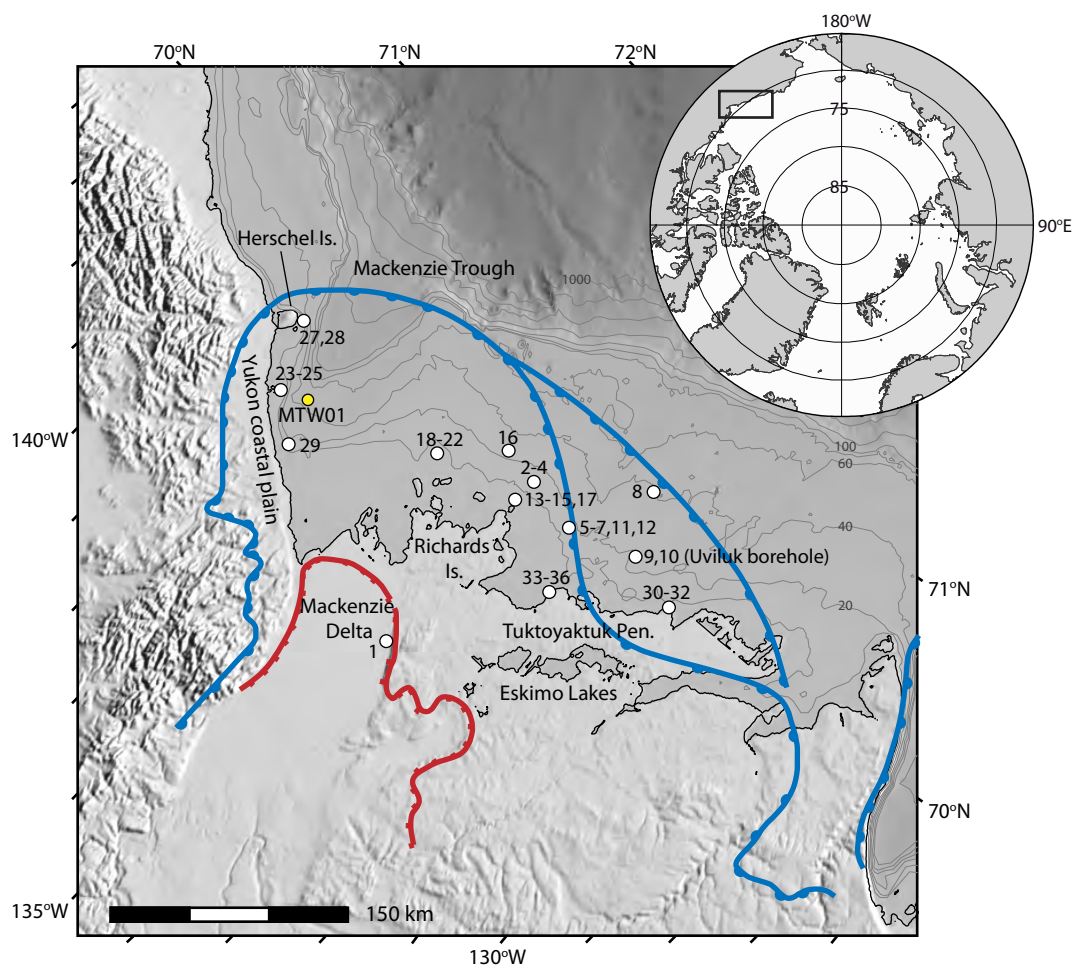
Map #	Site	Material	Depth (m b.s.l.)	¹⁴ C age and reported error (a BP)	Laboratory code	Median calibrated age (cal. a BP)	2σ calibrated age range (cal. a BP)
Terrestrial material							
1	NRC-Borehole	Wood fragment	38	6900±110	GSC-54	7750	7940 7570
2	BH2	Freshwater peat	24.8	6590±100	B-3033	7490	7660 7310
3	BH6	Freshwater peat	20.5	3740±70	B-3034	4100	4380 3890
4	BH4	Freshwater peaty clay	32.5	8300±90	B-3032	9290	9480 9030
5	VC-07	Freshwater peat	41.65	7740±90	B-4107	8530	8770 8370
6	VC-07	Freshwater peat	41.85	8820±100	B-4198	9890	10 180 9560
7	VC-07	Freshwater peat	41.92	8740±70	B-5068	9740	10 120 9540
8	NT-82-S01	Freshwater peaty clay	41.55	6000±70	B-6279	6840	7140 6670
9	UB-82-S23	Freshwater peaty clay	29.6	6640±80	B-6277	7520	7660 7420
10	UB-82-S23	Freshwater clayey peat	29.9	6310±100	B-6278	7230	7430 6990
11	AE-84-S101	Peat	45.15	7840±130	B-12233	8690	9000 8410
12	AD-84-S105	Freshwater peat	46.6	9910±150	B-12232	11430	12 010 10 820
13	BH34+00	Peat	23.6	5580±80	B-9504	6370	6550 6210
14	BH34+00	Wood fragments in peaty silt	23.75	6210±100	B-9507	7100	7410 6800
15	BH38+00	Plant debris in lacustrine silt	12.55	9470±100	B-9508	10760	11 140 10 440
16	KT-83-S02	Peat in fluvial sand	53.6	7730±160	B-9506	8560	9000 8210
17	BH15+00	Wood in marine sediments	20.5	3530±80	B-9501	3810	4070 3610
23	Babbage delta	Peat	0	2260±130	S-1482	2270	2710 1950
24	Babbage delta	Plant material in delta sediments	0	2110±90	GSC-2691	2100	2320 1900
25	Babbage delta	Peat	1.3	2100±80	GSC-2323	2080	2310 1900
26	Herschel Island	Charcoal in midden house	0.7	990±95	S-1533	900	1170 690
27	Herschel Island	Charcoal in midden house	0.7	1570±60	S-1532	1460	1600 1340
28	Herschel Island	Charcoal in midden house	0.7	1510±90	S-1534	1420	1600 1280
30	A3-87	Fresh water peat	0.2	2950±70	B-28281	3110	3340 2890
31	A2-87-100	Lagoonal, organic-rich silty sand	0.6	1280±70	B-28282	1210	1310 1010
32	A2-87-110	Freshwater peat	0.7	3820±90	B-28283	4220	4500 3930
33	C-88-1-20	Tidal-marsh (?) peat	0.5	1160±70	B-34307	1090	1260 940
34	C-88-1-46	Peat	0.3	2840±100	B-34308	2970	3210 2760
35	C-88-13-30	Peat	0.2	4920±220	B-34313	5660	6190 5050
36	C-88-12-B	Organic-rich silty clay	0.4	2690±80	B-34310	2810	3000 2520
Marine material							
29*	KF7, 9.4 m	Unidentified marine bivalve	29.4	3970±120	RIDDL_429	3570	3920 3180
18*	87NAH-39	Marine bivalves – <i>Portlandia frigida</i> fragments	7.3	1520±60	TO-1355	740	930 550
19*	87NAH-48	Marine bivalves – <i>Portlandia arctica</i> , <i>P. frigida</i> , <i>Cyrtodaria kurriana</i> , fragments	8.4	1460±50	TO-1356	690	880 530
20	87NAH-60	Marine bivalves – <i>C. kurriana</i> valves	10.8	2360±60	TO-1357	1590	1840 1350
21	87NAH-75	Marine bivalves – <i>C. kurriana</i> valves	8.6	1850±50	TO-1358	1070	1280 880
22	87NAH-81	Marine bivalves – <i>C. kurriana</i> fragments	8.6	1600±50	TO-1359	810	1010 640

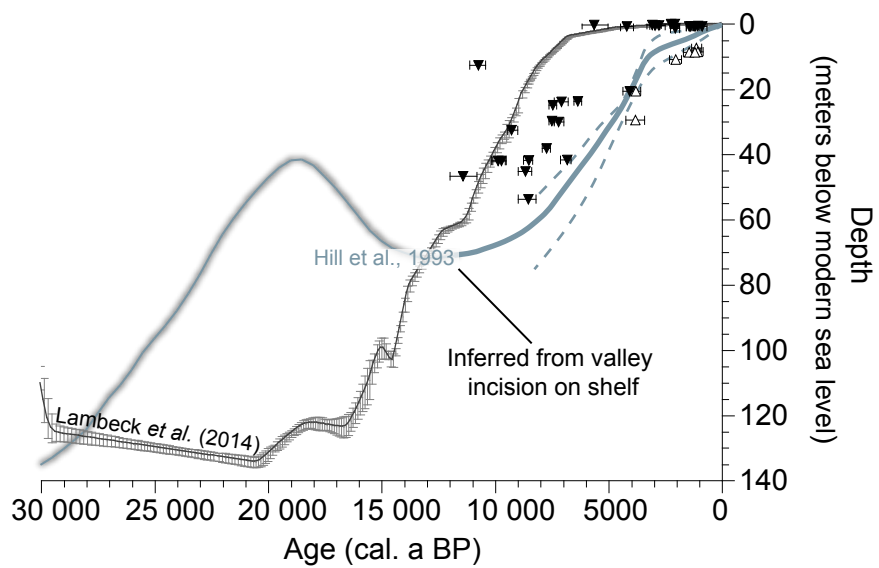
Table 2.

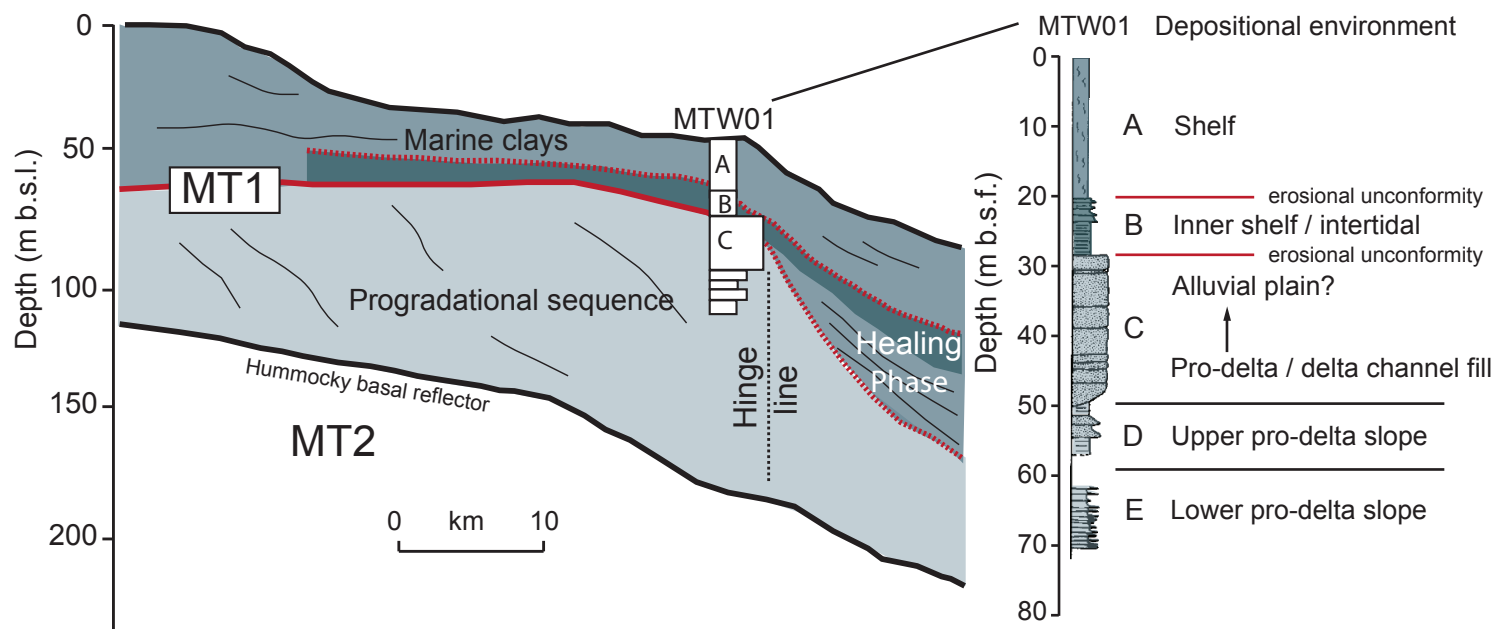
Sample	Unit	Type	Mid-Depth (m b.s.f.)	Range (+/- m)	Sample mass (mg)	¹⁴ C age (a BP)	1σ error	δ ¹³ C (‰)	Laboratory code	Median calibrated age (cal. a BP)	2σ calibrated age range (cal. a BP)		Modeled age (cal. a BP)	2σ modeled age range (cal. a BP)	
1A	A	MF	0.10	0.10	3.64	1570	20	-0.17	OS-103184	790	640	950	930	780	1080
1A	A	BF	0.10	0.10	6.92	1860	25	-1.40	OS-103002	1080	910	1260			
6B	A	MF	7.87	0.25	14.51	3910	30	1.15	OS-103003	3470	3240	3690	3560	3470	3800
6B	A	BF	7.87	0.25	4.02	4280	20	-1.62	OS-103185	3940	3680	4180			
12B	A	BF	17.17	0.25	4.2	7080	35	-0.91	OS-95351	7270	7060	7440	7050	6960	7380
14B	A	BF	20.02	0.20	3.58	8360	25	-1.34	OS-103186	8490	8310	8730	8320	8250	8530
15B	A	BF	20.91	0.18	4.4	8490	70	-0.89	OS-95606	8660	8400	8960	8470	8460	8810
16B	B	MF	21.82	0.18	7.1	9080	40	0.68	OS-95439	9400	9140	9580	Not modeled		

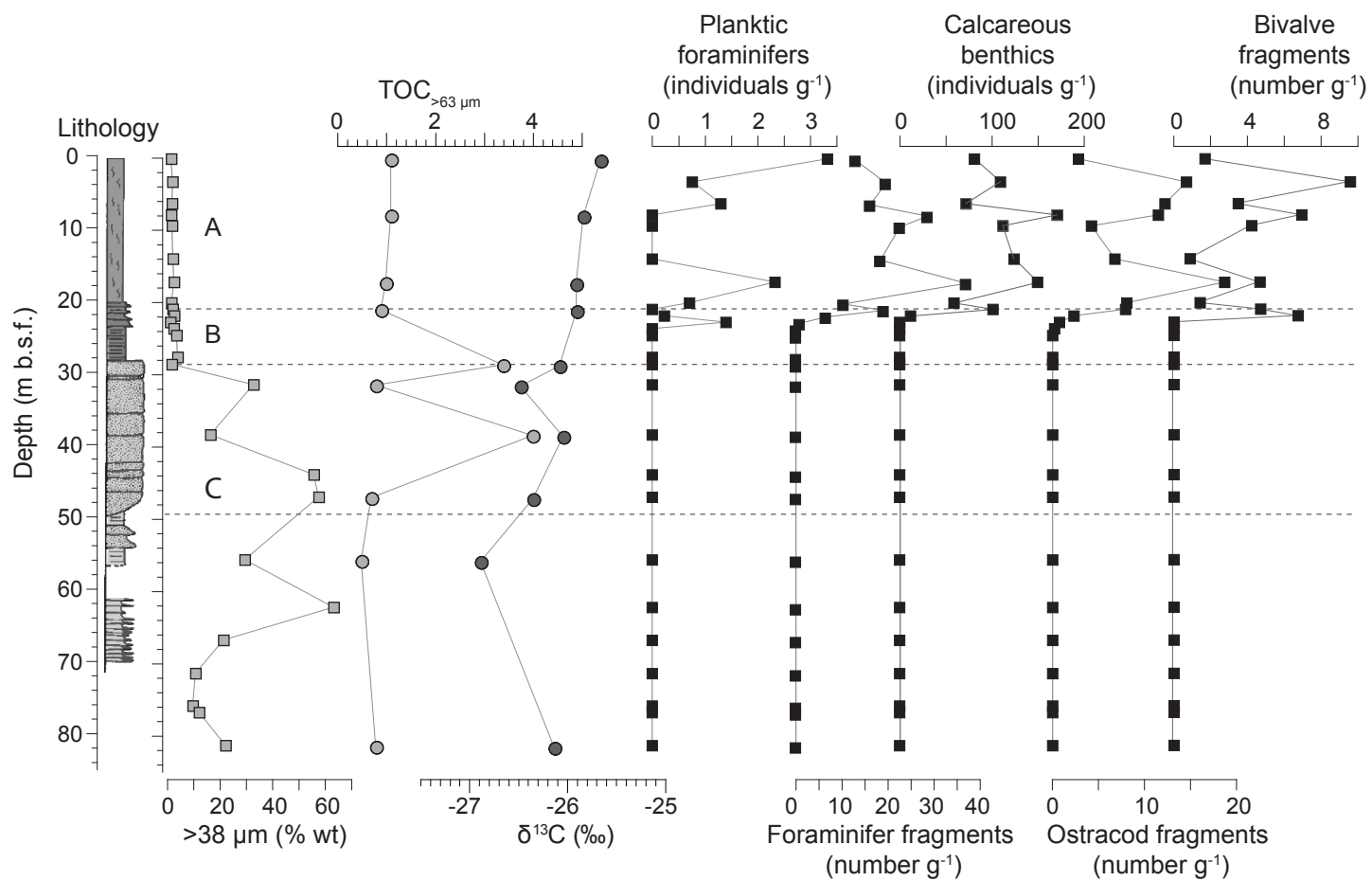
Table 3.

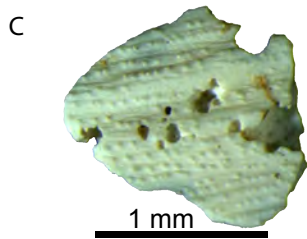
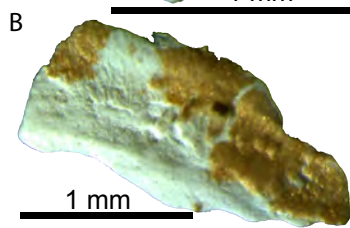
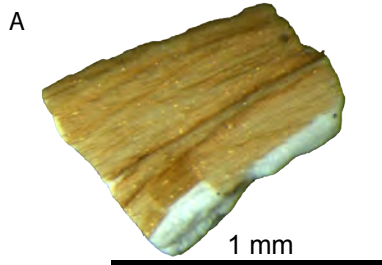
Sample	Unit	Mid-Depth (m b.s.f.)	Range (+/- m)	Carbon content (% wt.)	¹⁴ C age (a BP)	1 σ error	$\delta^{13}\text{C}$ (‰)	Laboratory code	Median calibrated age (cal. a BP)	2 σ calibrated age range (cal. a BP)	
1A	A	0.10	0.10	1.1	9608	44	-25.7	SUERC-43106	10 940	10 770	11 160
6B	A	7.87	0.25	1.1	11985	46	-25.8	SUERC-43108	13 830	13 730	14 000
12B	A	17.17	0.25	1	17031	72	-25.9	SUERC-43111	20 540	20 310	20 770
15B	A	20.91	0.18	0.9	17174	73	-25.9	SUERC-43113	20 710	20 500	20 940
21B	B	28.54	0.19	3.4	18595	100	-26.1	SUERC-42657	22 460	22 250	22 720
24B	C	31.35	0.20	0.8	24411	178	-26.5	SUERC-42659	28 440	28 000	28 810
28B	C	38.30	0.20	4	20818	109	-26.0	SUERC-43117	25 120	24 650	25 450
31B	C	46.91	0.27	0.7	22449	143	-26.4	SUERC-42661	26 770	26 340	27 180
35B	D/E	55.59	0.12	0.5	22924	150	-26.9	SUERC-42663	27 270	26 920	27 570
43B	E	81.29	0.21	0.8	20606	118	-26.1	SUERC-42667	24 820	24 440	25 210

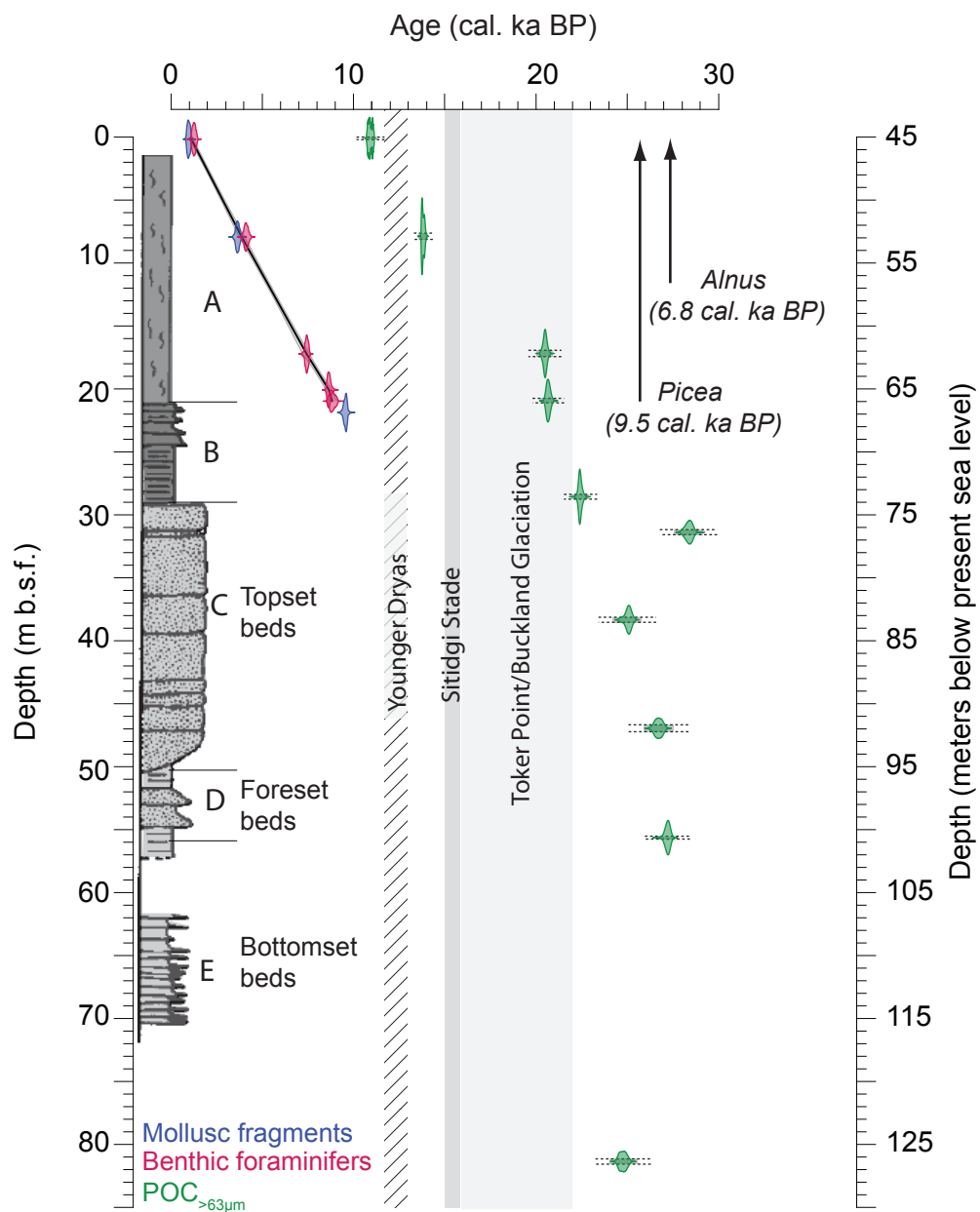


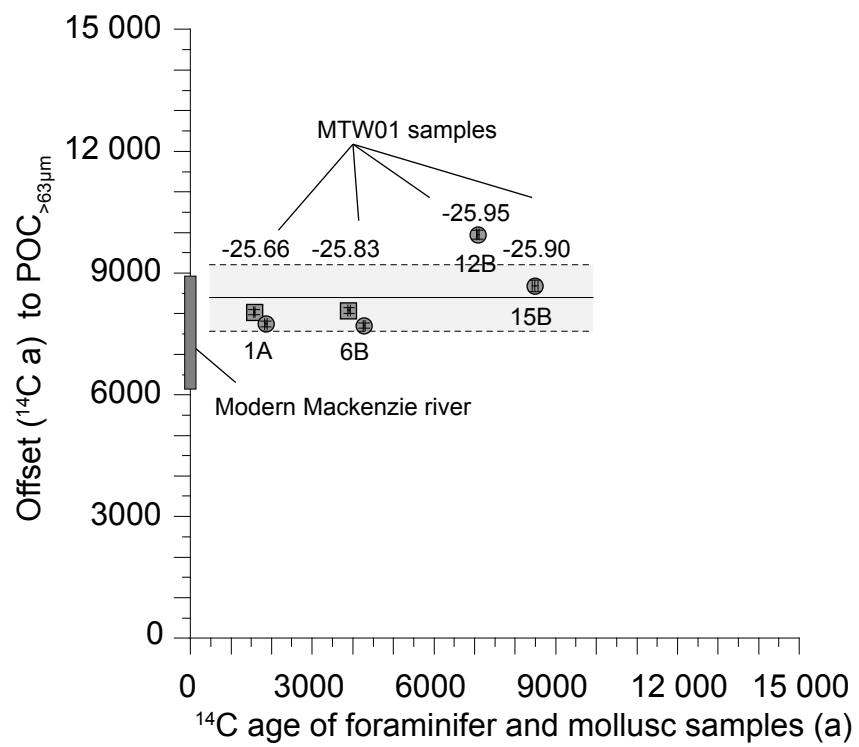


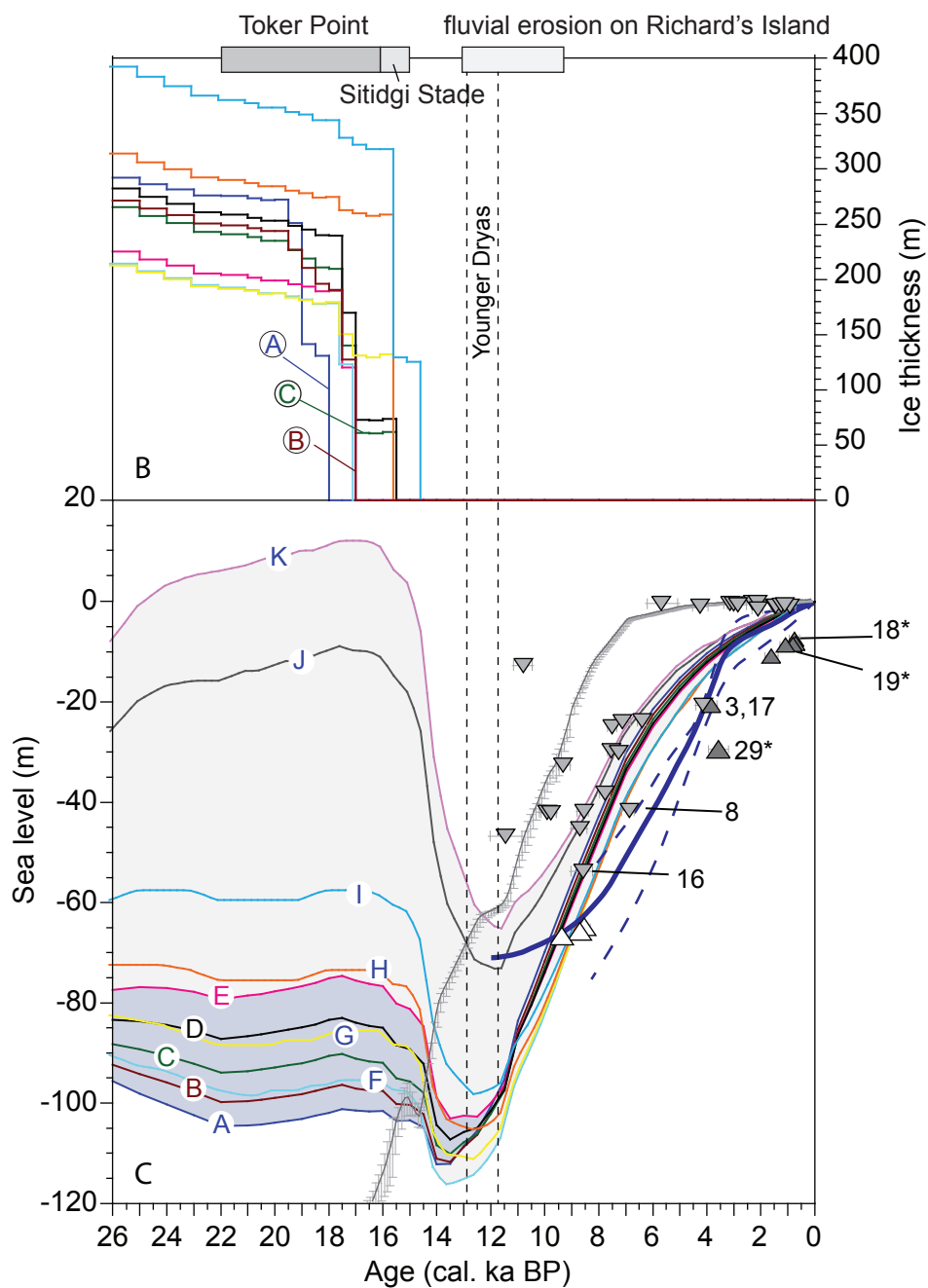
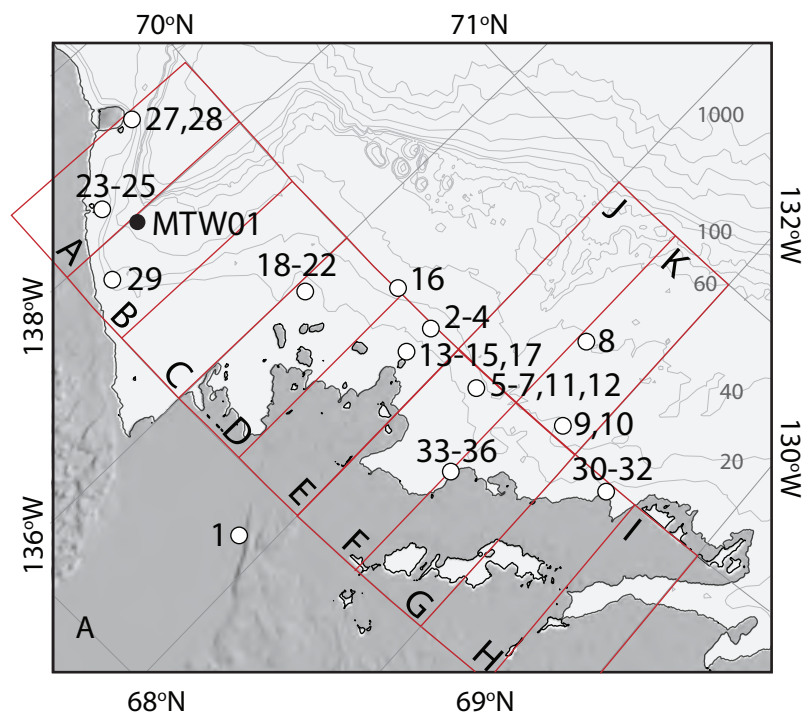












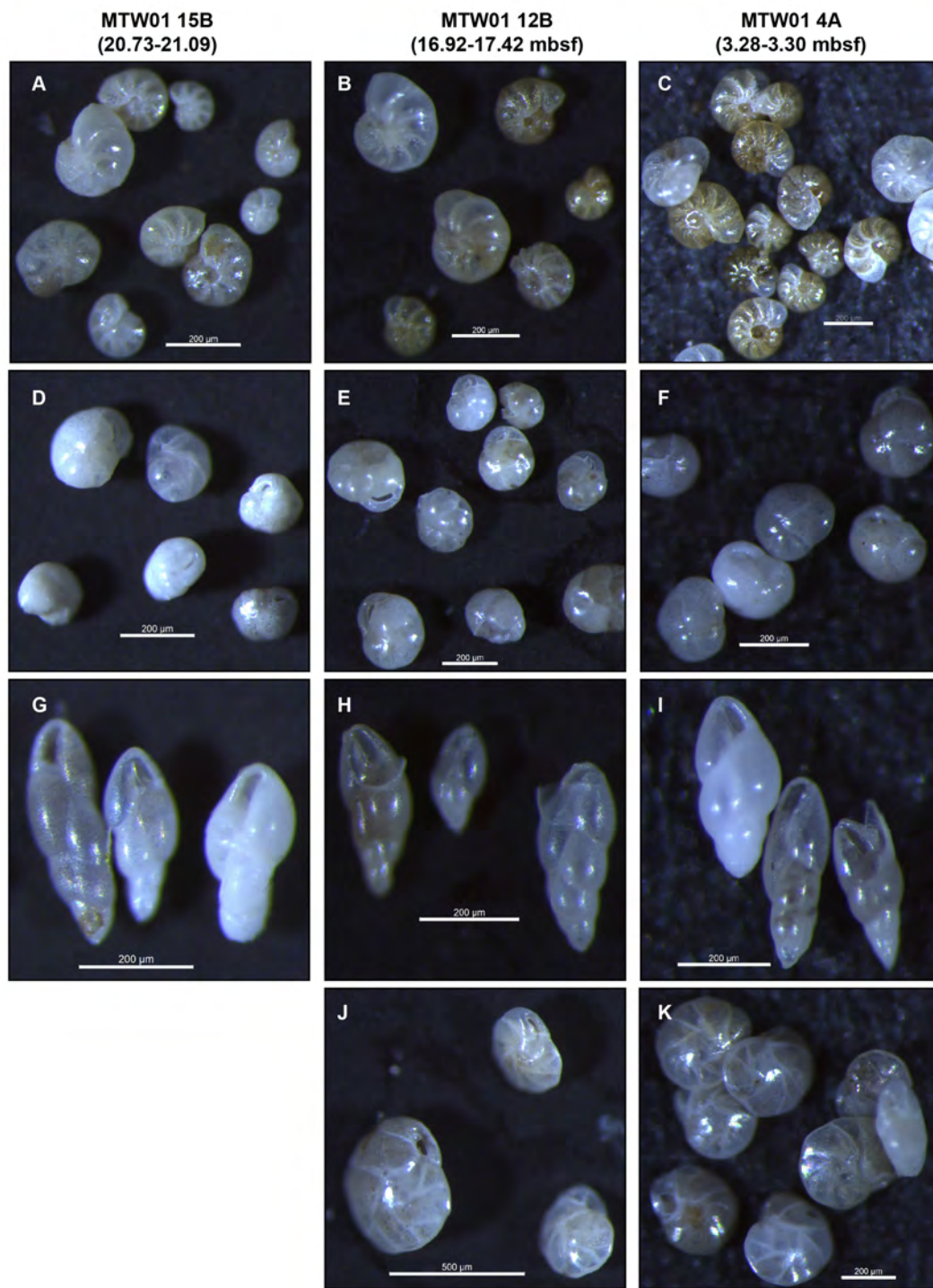


Figure S1. Photomicrographs of representative benthic foraminifera from MTW01 samples 15B, 12B and 4A. A-C: *Elphidium excavatum* subsp. *clavatum*, D-E: *Cassidulina reniformis*, G-I: *Bolivina arctica*, J-K: *Cassidulina teretis*. Scale bars are all 200 μm , except for J, which is 500 μm . Images were taken using a Leica M205 C microscope with camera system.

Table S1. Micro- and macrofossil content of samples from the MTW01 borehole.

Sample ID	Lithologic Unit	Top (m b.s.f.)	Bottom (m b.s.f.)	Mid dpeth (m b.s.f.)	Dry mass (g)	Dry mass (>38 µm) (g)	% wt >38 µm	Calc. benthic foraminifers (# in >63 µm fraction)	Planktonic foraminifers (# in >63 µm fraction)	Foraminifer fragments (# in >63 µm fraction)	Ostracod fragments (# in >63 µm fraction)	Mollusc fragments (# in >63 µm fraction)	Benthic Foraminifers (g ⁻¹)	Planktonic Foraminifers (g ⁻¹)	Foraminifer fragments (g ⁻¹)	Ostracod fragments (g ⁻¹)	Mollusc fragments (g ⁻¹)
1A	A	0.00	0.20	0.10	47.15	0.5	1.06	3691	157	609	132	79	81.4	3.3	12.9	2.8	1.7
4A	A	3.28	3.30	3.29	41.79	0.63	1.51	4400	32	816	608	400	109.5	0.8	19.5	14.5	9.6
5B	A	6.10	6.50	6.30	36.70	0.48	1.31	2592	48	592	448	128	72.4	1.3	16.1	12.2	3.5
6B	A	7.62	8.12	7.87	36.92	0.38	1.03	6136	0	1056	424	256	171.4	0.0	28.6	11.5	6.9
7B	A	9.14	9.61	9.38	43.67	0.58	1.33	4832	0	986	184	184	112.3	0.0	22.6	4.2	4.2
10B	A	13.72	14.18	13.95	36.62	0.61	1.67	4488	0	672	248	32	124.5	0.0	18.4	6.8	0.9
12B	A	16.92	17.42	17.17	41.13	0.84	2.04	6128	96	1520	768	192	149.8	2.3	37.0	18.7	4.7
14B	A	19.81	20.22	20.02	33.77	0.36	1.07	1968	24	348	272	48	59.2	0.7	10.3	8.1	1.4
15B	A	20.73	21.09	20.91	32.35	0.51	1.58	3216	0	616	256	152	101.6	0.0	19.0	7.9	4.7
16B	B	21.64	21.99	21.82	34.44	0.75	2.18	408	8	224	80	232	11.8	0.2	6.5	2.3	6.7
17B	B	22.56	22.85	22.71	39.89	0.27	0.68	0	56	32	30	0	0.0	1.4	0.8	0.8	0.0
18B	B	23.47	23.74	23.61	39.40	0.78	1.98	0	0	0	8	0	0.0	0.0	0.0	0.2	0.0
19A	B	24.38	24.66	24.52	38.45	1.16	3.02	0	0	0	0	0	0.0	0.0	0.0	0.0	0.0
20A	B	27.43	27.68	27.56	32.51	1.12	3.45	0	0	0	0	0	0.0	0.0	0.0	0.0	0.0
21B	B	28.35	28.73	28.54	40.46	0.49	1.21	0	0	0	0	0	0.0	0.0	0.0	0.0	0.0
24A	C	31.09	31.61	31.35	54.07	17.45	32.27	0	0	0	0	0	0.0	0.0	0.0	0.0	0.0
28B	C	38.10	38.50	38.30	32.16	5.12	15.92	0	0	0	0	0	0.0	0.0	0.0	0.0	0.0
30A	C	43.59	44.04	43.82	31.06	17.15	55.22	0	0	0	0	0	0.0	0.0	0.0	0.0	0.0
31B	C	46.63	47.18	46.91	41.92	23.91	57.04	0	0	0	0	0	0.0	0.0	0.0	0.0	0.0
35B	D	55.47	55.70	55.59	37.46	10.85	28.96	0	0	0	0	0	0.0	0.0	0.0	0.0	0.0
37A	E	61.87	62.47	62.17	39.27	24.64	62.75	0	0	0	0	0	0.0	0.0	0.0	0.0	0.0
39B	E	66.45	66.95	66.70	36.88	7.71	20.91	0	1	1	1	1	0.0	0.0	0.0	0.0	0.0
40B	E	71.02	71.60	71.31	31.45	3.21	10.21	0	0	0	0	0	0.0	0.0	0.0	0.0	0.0
41	E	75.59	76.00	75.80	49.69	4.54	9.14	0	0	0	0	0	0.0	0.0	0.0	0.0	0.0
42	E	76.50	76.95	76.73	27.09	3.13	11.55	0	0	0	0	0	0.0	0.0	0.0	0.0	0.0
43B	E	81.08	81.50	81.29	91.13	19.75	21.67	0	0	0	0	0	0.0	0.0	0.0	0.0	0.0